Dye-Sensitized DNA Photocleavage Facilitated by Donor-Acceptor Fluorophores in the NIR Wavelength Range

Dye-Sensitized DNA Photocleavage Facilitated by Donor-Acceptor Fluorophores in the NIR Wavelength Range

by

Carine Seudieu

Under the Direction of Kathryn B. Grant, PhD

A Thesis Submitted in Partial Fulfillment of the Requirements for the Degree of

Master of Science

in the College of Arts and Sciences

Georgia State University

2022

ABSTRACT

We report the DNA photocleavage abilities of **GEO30** and **GEO31,** near-infrared (NIR) donor-π-acceptor fluorophores (D-π-A) with a chloroacrylic acid acceptor linked to an indole donor group via a π-conjugated linker containing a cyclohexene and a *meso*-chlorine atom. We are interested in developing these fluorophores as NIR photosensitizers (PS) in photodynamic therapy (PDT). UV-visible spectrophotometry studies showed that **GEO30** and **GEO31** were unstable in aqueous buffer but exhibited stable DNA interactions. Competitive DNA binding results using pentamidine and methyl green indicated that dyes **GEO30** and **GEO31** possibly bind in the minor and major grooves of DNA. In the absence and presence of a fluorescent probe and chemical additives, the irradiation of the dyes with a 750 nm LED medical lamp was shown to generate Type I hydroxyl radicals that formed direct DNA cleavage in high yields (pH 7.0, 10 °C).

INDEX WORDS: D-π-A fluorophores, PDT, NIR, UV-visible spectrophotometry, Groove binding, Photocleavage, Hydroxyl radicals, Fluorescent probes, Chemical additives

Dye-Sensitized DNA Photocleavage Facilitated by Donor Acceptor Fluorophores in the NIR Wavelength Range

by

Carine Seudieu

Committee Chair: Kathryn B. Grant

Committee: Samer Gozem

Dabney Dixon

Electronic Version Approved:

Office of Graduate Services

College of Arts and Sciences

Georgia State University

August 2022

DEDICATION

This thesis is dedicated to both my father, Dieudonne Seudieu, and my mother, Marie Ndongmo, for their unwavering love and support throughout my life. I am grateful for all of the sacrifices they have made to help me get to where I am today. To my siblings, uncles, and aunts, I thank them for their support, encouragement, and thoughtfulness throughout my life. To my father, I thank you for teaching me the importance of a good education and to never give up on my dreams. You taught me to be resilient in the face of adversity. Thank you for that because it has given me the strength to be where I am in my academic career and complete this masters research. To my mother, you are a fighter and an incredibly strong and independent woman. For that, I salute you and give you my utmost respect. You taught me the importance of independence and how being a woman in a field dominated by men is a strength, not a weakness. Lastly, I would like to express my gratitude to every one of my friends for all of the wonderful memories and words of support you all have given me throughout my master's program.

ACKNOWLEDGEMENTS

I want to express my gratitude to everyone who helped me achieve this master's degree. I especially want to express my gratitude to Dr. Kathryn Grant for all of her assistance and words of encourage throughout this master thesis journey. You were an amazing advisor and I learned tremendously under your direction. I appreciate how welcoming you were and how you would take the time to get to know us personally. I would also like to give a special thanks to Dr. Henary and Guliz Ozmen for synthesizing the compounds used in this thesis. Furthermore, I would like to thank Dr. Dabney Dixon and Dr. Samer Gozem for agreeing to be part of my thesis committee and the Chemistry Department at Georgia State University for their support and the research opportunity they gave me. To my friend David Brewer, I appreciate your support, guidance, and word of encouragement to help me complete this thesis. Lastly, I would like to thank all my lab mates Aikohi Ugboya, Karen Phan, and Erhunmwense Obayuwana for making the lab exciting and unforgettable.

TABLE OF CONTENTS

LIST OF FIGURES

LIST OF ABBREVIATIONS

CT DNA	=	Calf thymus DNA
D_2O	=	Deuterium oxide
D-π-A	=	Donor-π-Acceptor Fluorophore
EDTA	=	Ethylenediaminetetraacetic acid
EtBr	=	Ethidium bromide
HpD	=	Hematoporphyrin
HPF	=	Hydroxyphenyl fluorescein
ICT	=	Intramolecular charge transfer
LED	=	Light emitting diode
NIR	=	Near infrared
PDT	=	Photodynamic therapy
PS	=	Photosensitizer
ROS	=	Reactive oxygen species
UV	=	Ultraviolet

1 A THERAPEUTIC APPROACH WITH PHOTODYNAMIC THERAPY: DNA PHOTOCLEAVAGE AND DNA-FLUORPHORE DYE INTERACTIONS

1.1 Photodynamic Therapy

Photodynamic therapy (PDT) is a type of phototherapy used to treat a variety of diseases, such as cancer. PDT is a technique that involves administering a photosensitizer (PS) via topical, oral, or intravenous routes.[1,2] PS in target tissues is activated by light to form highly localized reactive oxygen species (ROS). PDT can be used before and after radiation therapy or chemotherapy, and unlike most traditional treatments, it is non-invasive and generates less cytotoxicity.[3,4] PDT can accurately target the afflicted tissue without damaging healthy cells in neighboring areas. Therefore, this procedure is promising because it has few adverse effects and can be used repeatably.[5] PDT was first reported to treat non-Hodgkin lymphoma, especially cutaneous T-cell lymphoma and a variety of skin conditions.[6, 7] Subsequently, it has been shown to be a promising treatment for malignant tumors of the esophagus, skin, head, neck and bladder.[8,9] Researchers have discovered that the combination of chemotherapy and PDT improves the survival rates of certain cancers including stage III and IV non-small cell lung cancer (NSCLC).[9]

PDT is employed in urology, dermatology, gastrointestinal, dentistry, and among other specialties.[10] Due to the broad applications of PDT, this procedure is often used in dentistry for periodontal care or utilized to sterilize the oral and dentin tissues.[11, 12]

1.1.1 Photodynamic Therapy: A Brief History

Phototherapy was first used to treat diseases such as vitiligo, psoriasis, and rickets.[13] Niels Finsen, a Danish scientist and physician, advanced phototherapy research by experimenting with various light sources to treat a variety of medical conditions. The studies he conducted earned him the Nobel Peace Prize in 1903 for his use of carbon arc phototherapy to treat skin tuberculosis.[14]

Other scientists, such as von Tappeiner, were inspired by his work to employ light as a therapeutic mechanism. He was the first researcher to treat basal cell carcinoma using dyes in combination with an arc-lamp or sunlight exposure.[15, 16] He additionally applied light and dyes to treat tumors, syphilis, and tuberculosis, thus coining the term "photodynamic therapy" after he observed that oxygen was one of the primary criteria of the treatment.[17, 18]

In 1960, Mayo Clinic's Schwartz and Lipson discovered the hematoporphyrin derivative (HpD), a porphyrin-based photosensitizer, while conducting PDT research.[19] It was observed that after injecting hematoporphyrin during surgery, the phototoxic effects and fluorescence of neoplastic lesions were elevated.[20] In the 1970s, Dowerty studied the translational importance of PDT as a treatment for a variety of cancers using HpD, which beams highly localized in tumors.[19, 21] A few years later, in 1993, the first officially approved PDT drug, porfimer sodium, was developed in Canada to treat bladder disease.[21] Many other derivatives of porfimer sodium have been synthetized since its initial discovery as a PS agent. As a result, many PS agents have been approved worldwide for use in imaging, the treatment of cancer and other medical conditions.

1.2 PDT's Principle and Components

The PDT technique entails introducing a PS into targeted tissues. The procedure consists of two phases: first, the PS is administered in the afflicted tissues and accumulates and second, the PS is activated by exposure to low intensity light of a specific wavelength.[22] The main components of PDT are light, PS, and oxygen.[23] Each component is important in PDT treatment, thus choosing the appropriate components is essential for its effective therapy.

1.2.1 Photosensitizing Agents

A PS needs to be water-soluble, free of toxic contaminants, stable, and able to absorb light that can pass through living tissues.[24] For optimal tissue penetration, the absorbed light should be

in a "therapeutic window", which is the infrared wavelength range of 700-900 nm that allows deep passage of light through the blood and skin.[25, 26] Ideally, the PS should accumulate in target cells, exhibit negligible toxicity in the dark, and produce significant cytotoxic effects upon photoactivation by effectively producing reactive oxygen species (ROS).[27] In order to administer an effective PDT treatment, the PS must have a high quantum yield and extinction coefficient.[28] In addition, there must be an appropriate PS concentration for uptake in tumor tissues.[29, 30] Differences in light transmission, PS type, and oxygen permeability in different tissues can make it difficult to predict the effects of PDT.[31]

Photosensitizers can behave as antibacterial or anti-cancer drugs. Antibacterial photosensitizers tend to have a significant cationic charge and are excellent agents for gram-negative bacteria. In contrast, most anti-cancer photosensitizers are lipophilic and have a neutral or low overall charge.[32] Photosensitizers with tetrapyrrole groups based on bacteriochlorophyll, chlorophyll, and heme are the most common PS types of photosensitizers used in cancer treatment. The four main categories of this type of tetrapyrrole photosensitizers are chlorin, bacteriochlorin, porphyrins and phthalocyanines. Groups of new photosensitizers under development include synthetic transition metal complexes, phenothiazinium and cyanine dyes.[33] Photofrin is one of the first FDA-approved PDT drug used worldwide. In the United States, the FDA has approved porfimer sodium, methyl aminolevulinate, and verteporfin. Porfimer sodium was approved for the treatment of Barrett's esophagus, and outside of the U.S, temoporfin for the treatment of neck and head cancers, and talaporfin for lung cancer. [34, 35]

1.2.2 Light Sources

A suitable light source is required to activate PS agents. The light source should have a wavelength that matches light absorption by the PS.[36] The selected light source must also have a

wavelength in the therapeutic window. This is because the energy in this region is sufficient to drive the ground state PS into an excited state, as well as allowing for deep light penetration through biological tissues. Lasers, lamps, and light-emitting diodes (LEDs) are PDT applications' most commonly used light sources. Other notable light sources employed in PDT are metal vapor lasers, argon-dye laser systems, potassium titanyl phosphate (KTP)-dye lasers, and carbon dioxide lasers (CO_2). [37, 38]

Lasers are more efficient than other light sources because they are administered directly and precisely via fiber optic cables to transmit light to damaged cells in the human body. In addition, lasers produce light with easily recognizable monochromatic wavelengths and high PS photoactivation efficiencies of over 90%.[39] For many PDT applications, diode lasers are the preferred light source. This is because they act as semiconductors and do not require optical assembly, unlike traditional lasers. Diode lasers are compact, affordable, and easy to set up.[40] In contrast, CO_2 lasers treat tumors such as Bowen's disease, squamous cell carcinoma, and basal cell carcinoma by excision or vaporization.[41, 42] Alternatively, LEDs have been used in PDT for many years due to their portability, low energy, and high light output. LEDs produce light by luminescence, which is measured electronically.[43]

When implementing the PDT method, it is necessary to study the properties and situations affecting the selected light source. This includes investigating the location of the disease and the type of PS. Due to limited light depth, some PS and light sources are ineffective for PDT operation. Therefore, PDT is more efficient for minor skin lesions and early stage, light accessible cancers.

1.3 PDT Mechanism of Action

A PDT reaction induces a biological response, damaging specifically targeted tissues. Initially, the PS is in its singlet ground state. Upon absorption of a photon, PS transitions from the singlet

ground state S_0 to an S_1 singlet excited state. In the S_1, the PS has several ways to relax. The PS lose energy by emitting light (fluorescence) or to generate heat by internal conversion.[44] Singlet excited-state PS can undergo a spin inversion via the intersystem crossing (ISC) process to achieve a lower energy triplet state (T_1) with unpaired electrons.[31] In the excited triplet state, the PS (^{3}PS*) can either release photons via phosphorescence to return to its ground state or undergo a PDT reaction. The T_1 state has a longer lifetime than S_1 allowing the photosensitizers to interact with molecules.[45] In the proximity of ground state triplet oxygen ($^3O_2$), the ^{3}PS* generates ROS via electron transfer (Type I) or energy transfer (Type II) mechanisms (Figure 1.1).

In Type I electron transfer, the ^{3}PS* interacts with neighboring molecules by donating or accepting electrons. Upon electron donation, the superoxide anion radical ($O_2^{\bullet-}$) is produced when the triplet state photosensitizer anion radical ($^3PS^{\bullet-*}$) combines with $^3O_2$.[46, 47] The spontaneous dismutation of superoxide anion radicals produces hydrogen peroxide (H_2O_2), which gives rise to hydroxyl radicals ($^{\bullet}OH$) by oxidizing (Fe^{2+}) via Fenton chemistry (Figure 1.3)[48, 49, 50] The hydroxyl radicals have a short lifetime and are highly reactive. Therefore, they react with biomolecules nearby due to their high positive redox potential and unpaired electron.[51, 52] In contrast, by the Type II pathway, highly reactive singlet oxygen ($^1O_2$) is formed through the energy transfer from the excited triplet state ^{3}PS*. Due to $^1O_2$ having a short lifetime in cells, its cellular targets are only those regions with high PS accumulation.[53]

Type I and Type II processes can both cause oxidative damage to macromolecules, including the nucleic acid, proteins, and lipids.[54] The primary cause of tumor tissue death in PDT is through Type II energy transfer pathway. ROS induce oxidative damage to DNA through alkali-labile lesions or single-strand break (SSB). As a result, this damage to biological molecules causes apoptotic or neucrotic cell death in targeted tissues.[55]

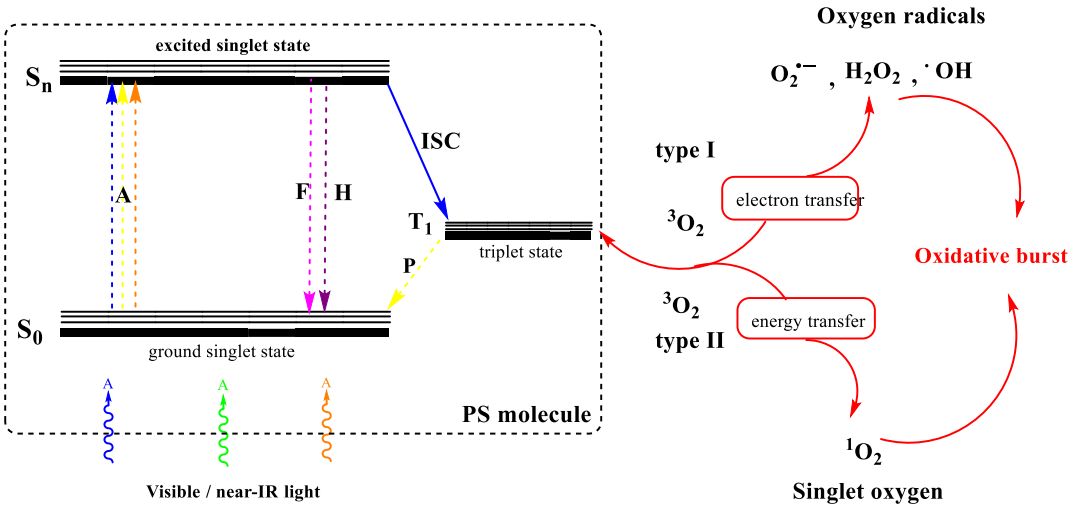

Figure 1: Jablonski diagram illustrating Type1 and Type 2 PDT mechanisms. Abbreviations: A, absorbance; F, fluorescence; H, internal conversion; ISC, intersystem crossing; P, phosphorescence.

$$(1)\quad {}^3PS^{\bullet-*} + {}^3O_2 \longrightarrow {}^3PS^{*} + O_2^{\bullet-}$$

$$(2)\quad Fe^{3+} + O_2^{\bullet-} \longrightarrow Fe^{2+} + O_2$$

$$(3)\quad 2O_2^{\bullet-} + 2H^{+} \longrightarrow H_2O_2 + {}^3O_2$$

$$(4)\quad Fe^{2+} + H_2O_2 \longrightarrow Fe^{3+} + {}^{\cdot}OH + OH^{-}$$

Figure 2: Fenton reaction mechanism depicting the formation of hydroxyl radicals.

1.3.1 Routes of Tissue Destruction

PDT has been shown to target tumor cell lysosomes, the endoplasmic reticulum (ER), nuclei, plasma membranes, and mitochondria.[56] Tumor cells are damaged in two ways: necrosis (unprogrammed cell death) and apoptotic (programmed cell death).[57, 58] In necrosis, cell death is caused by physical or toxic trauma that induces the swelling of the endoplasmic reticulum,

mitochondria, and plasma membrane causing the organelles and cells to burst and release their contents into the surrounding environment.[59]

Apoptosis is the most common form of cell death in PDT.[60.] Apoptosis occurs when cells respond to internal or external stimuli, resulting in physical and biochemical modifications. Activation of hydrolases such as proteases and nucleases regulates apoptosis, causing DNA strand breaks and changes inside organelles.[61, 62] Inflammatory cytokine tumor necrosis factor (TNF) is involved in cell survival, development, proliferation, and death.[63] TNF stimulates cell surface receptors that activate caspase-8 via scaffolding proteins during apoptosis.[64, 65] Caspase-8 activates downstream caspases such as caspase-3 and causes cells to undergo apoptosis.[66] In humans, about two-thirds of caspases are involved in apoptosis.

1.4 The Production of Reactive Oxygen Species

ROS are naturally produced as a by-product of photosynthesis, cell respiration, electron transport chain in mitochondria and by the cytoplasmic membrane nicotinamide adenine dinucleotide phosphate (NADPH) oxidase. ROS are essential in cell signaling, metabolism, memory development, and homeostasis under physiological conditions.[67] In addition, ROS can originate from both intrinsic and extrinsic sources.

1.4.1 The Production of Intrinsic ROS

ROS are formed in human cells primarily by the mitochondrial via the electron transport chain and enzymes from cytoplasmic membrane nicotinamide adenine dinucleotide phosphate (NADPH) oxidase.[68] Triplet ground state oxygen ($^3O_2$) is intracellularly predominant and causes the formation of ROS in the cell, allowing oxygen to accept electrons from the oxidative pathway.[69] In photosynthesis, plants produce ROS when triplet-excited state oxygen is converted

to $^1O_2$ in the presence of sunlight, chlorophyll, and oxygen. In *Arabidopsis* thaliana cells with elevated light levels, $^1O_2$ was shown to be the most abundant.[70]

1.4.2 The Production of Extrinsic ROS

Environmental contaminants, sunlight exposure of nitrites (NO_2) and nitrates (NO^{3-}), heavy metals, and some medications, such as gentamycin, gentamycin, and cyclosporine have been reported to all produce ROS.[71, 72] In addition, ozone (O_3) and chlorophyll can undergo a process in which O_3 functions as an electron acceptor, acquiring electrons from photoexcited chlorophyll to produce •OH.[72] As previously stated, photodegradation via Type I and II pathways are causes of ROS formation.

1.5 Adverse Effects of ROS

ROS buildup is detrimental to biomolecules as it can lead to a number of diseases by promoting oxidative stress.[72] Oxidative stress arises when there is an imbalance between ROS generation and antioxidative defenses. As a result, as oxidative stress builds up, macromolecules such as lipids, nucleic acids, and proteins undergo oxidative damage.[73] Oxidative stress has a detrimental effect by generating mutagenic 8 hydroxy 2-deoxyguanosine (8oxodG) and deoxythioguanosine (dTG) DNA nucleotides. Under free radical damage and UV light exposure, the oxidized nucleotides have been reported to be elevated in the body.[73]

1.6 ROS Cellular Defense Mechanism

Under aerobic conditions, cellular detoxification is critical for cell survival. Whether ROS functions as a signaling molecule or induce oxidative damage by free radicals depends on the balance between ROS and antioxidant levels.[74] ROS levels are regulated intracellularly by both enzymatic and non-enzymatic processes. The most significant enzymes of the cell antioxidant defense system are glutathione peroxidase, superoxide dismutase (SOD), and catalase.[75] Non-

enzymatic antioxidants that reduce ROS levels are vitamin E, vitamin C, vitamin A, selenium (Se), transferrin, and glutathione (GSH).[76]

SOD initiates detoxification processes by catalyzing the dismutation of superoxide anion radicals to H_2O_2.[75] Catalase is a prevalent enzyme found in the peroxisome that catalyzes the breakdown of the hydrogen peroxide to water and oxygen in nearly all living organisms exposed to oxygen.[75] Glutathione peroxidase, a selenium-containing enzyme, catalyzes the detoxification of hydrogen peroxide and hydroperoxides to alcohols by reduced glutathione.[77] Glutathione is found in two forms: oxidized glutathione disulfide (GSSG) and reduced glutathione (GSH).[77] GSH is a tripeptide composed of cysteine, glutamic acid, and glycine. It is known for its role in intracellular defense against ROS and free radical toxicity.

1.7 DNA Interaction with Small Molecules

Current chemotherapy against some cancers, as well as parasitic, and viral diseases can involve nucleic acids interacting reversibly or irreversibly with small molecule drugs and dyes. Drugs bind to nucleic acid via three reversible non-covalent modes: external electrostatic, groove binding (minor and major), and by intercalation (Figure 1.3).

1.7.1 Intercalation

Intercalators through π-π stacking interactions stack between DNA base pairs about 3.4 Å apart.[78] By increasing this rise, the helix of the DNA is lengthened, allowing intercalating molecules to be incorporated into the DNA.[79] Small compounds with a planar aromatic ring systems can be inserted between the hydrophobic regions of DNA base pairs.[79] The main driving forces of intercalation are the base pair π-π stacking interactions, while hydrogen bonds and electrostatic forces provide additional stabilization.[80, 81]

Intercalators can increase DNA viscosity upon binding by increasing rise which elongate the double-stranded DNA.[82] Well reported compounds, such as ethidium bromide (EtBr), methylene blue, acridine orange, and polycyclic aromatic hydrocarbons (PAHs), have been found to insert themselves between the planar bases of DNA.[82, 83] In addition, intercalators such as daunorubicin, and adriamycin have been reported to inhibit DNA replication in cancer cells; compounds intercalate in-between DNA base pairs.

1.7.2 Groove Binders

Groove-binding interactions occur when a small molecule interacts directly with the walls and base pair edges in the grooves of nucleic acid. Grove binding can involve the major and minor grooves that differ in terms of hydrogen bonding interactions, steric effects, electrostatic potentials, and degrees of hydration. Small molecules prefer to bind in the minor groove of DNA. These small molecules usually have aromatic rings connected through flexible bonds, which allow for torsional rotation to fit the helical curvature of the groove with the water molecules being displaced. These cationic molecules with unfused aromatic rings include pentamidine, netropsin, and distamycin all bind to the minor groove of DNA.[83, 84] In groove-binding interactions, DNA can undergo structural transitions during complex formation; the interactions are stabilized by van der Waals interactions and hydrogen-bonding with the groove binder.[85] Most minor groove binders bind to narrow AT-rich DNA sequences because they have narrow minor grooves, while intercalators prefer to bind to GC-rich sequences because they enhance π-π stacking interaction .[85, 86]

1.7.3 Electrostatic and External Binders

Due to the negatively charged sugar phosphate backbone of double-stranded DNA, external DNA binders, including cations such as sodium ion (Na^+) and magnesium ion (Mg^{2+}) can modify the DNA structure when they bind. The negatively charged phosphate oxygen atoms in the

DNA backbone and the cationic part of the binder interact electrostatically, thus inducing external binding.[87]

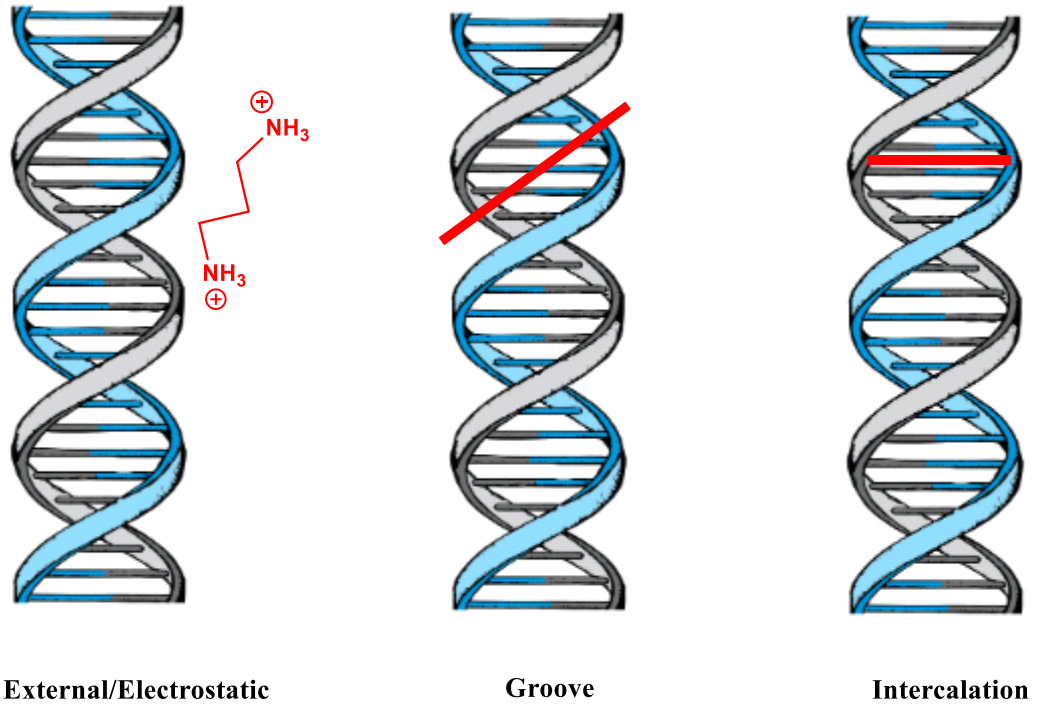

Figure 3: The three ways small molecules can reversibly bind to double-helical nucleic acids.

1.8 DNA Photocleavage

Photocleavage of DNA is process that oxidizes nucleobases or sugar residues, causing nucleotide degradation and DNA fragmentation.[87] It has been reported that some chromophores can induce dye-sensitized DNA cleavage by generating hydroxyl radicals upon light absorption, which then abstract hydrogen atoms from deoxyribose.[90] DNA cleavage can also be induced directly by singlet oxygen. Damaged plasmid DNA fragments caused by generating hydroxyl radicals or singlet oxygen can be separated and examined *in vitro* using agarose gel electrophoresis.[91, 92]

The three types of DNA bands shown on an agarose gel are supercoiled, nicked, and linear. The supercoil form is a native plasmid DNA conformation caused by an overtwist of the double helical strands. Nicked DNA is the relaxed form of the supercoiled conformation, in which DNA breakage occurs at distinct sites on the same or opposite DNA strand. In the linear form, DNA breaks occur at the same site on opposite DNA strand. The photocleavage effectiveness is highly dependent on the PS binding mechanism and affinity for DNA.[96]

1.9 Photonucleases

Researchers have extensively studied photonucleases also known as DNA photocleaving agents due to their potential therapeutic advantages in PDT.[96] Photonucleases are molecules that directly bind to DNA and cause the breakage of dsDNA when irradiated with a light source. Photonucleases are divided into two types: metal complexes and organic dyes.[34] DNA photocleavage has been proven when bivalent metals such as iron(II), copper(II), cobalt(II), zinc(II), or nickel(II) are introduced into metal complexes. Metal cations have also been found in various anticancer drugs, which exhibit therapeutic efficiency. Other metal complex photosensitizers incorporating ruthenium(II), platinum(IV), ruthenium(II), iridium(III), and rhodium(III) have been studied [97-102] Although some metal-based photonucleases have been shown to be promising therapeutic agents, many metals in pharmaceuticals drugs have the potential to be toxic. This is because the metal ions can dissociate from the photonuclease and interfere with biological activities.[97] For this reason, organic dyes such as anthraquinones, cyanines, and donor-π-acceptor fluorophores have been studied for their ability to photocleave DNA strands.

1.10 Donor Acceptor Fluorophores

Donor–π-acceptor (D–π-A) fluorophores are a class of synthetic organic dyes that have piqued the interest of scientists due to their push-pull mechanism.[98] This class of fluorophores has a donor

and acceptor moiety coupled by a conjugated π linker (Figure 1.4).[98] The push–pull process is facilitated by this conjugation, where the donor group "push" and the acceptor group "pull" the electrons, leading to intramolecular charge transfer (ICT) upon light absorption.[98] The fluorescence characteristics of the molecules can be tuned from UV-visible to NIR by combining appropriate electron donor and acceptor units.[98] The NIR region is useful for biological imaging because light can penetrate deeper into with low autofluorescence from molecules in the body.[99] Nonlinear optical imaging, organic light emitting diodes (OLEDs), dye-sensitized solar cells (DSCs), and biosensors are all applications for NIR donor acceptor fluorophores.[100-103] Furthermore, because of their biological and photochemical potential, near-infrared (NIR) D–π-A push–pull fluorophores are being employed as photosensitizing agents in our research on NIR DNA photonucleases. Fluorophores synthesized by our collaborator GSU professor Maged Henary contain a chloroacrylic acid acceptor coupled to a Vilsmeier–Haack linker with a chlorocyclohexene and donor moieties indole, benzothiazole, and quinoline (Figure 1.4). Donor acceptor fluorophores can potentially bind externally, in a groove, or intercalate into DNA based on the structure of the dye. When DNA interacts with dye, the DNA-dye interaction can result in a change in the dye's aggregation state.

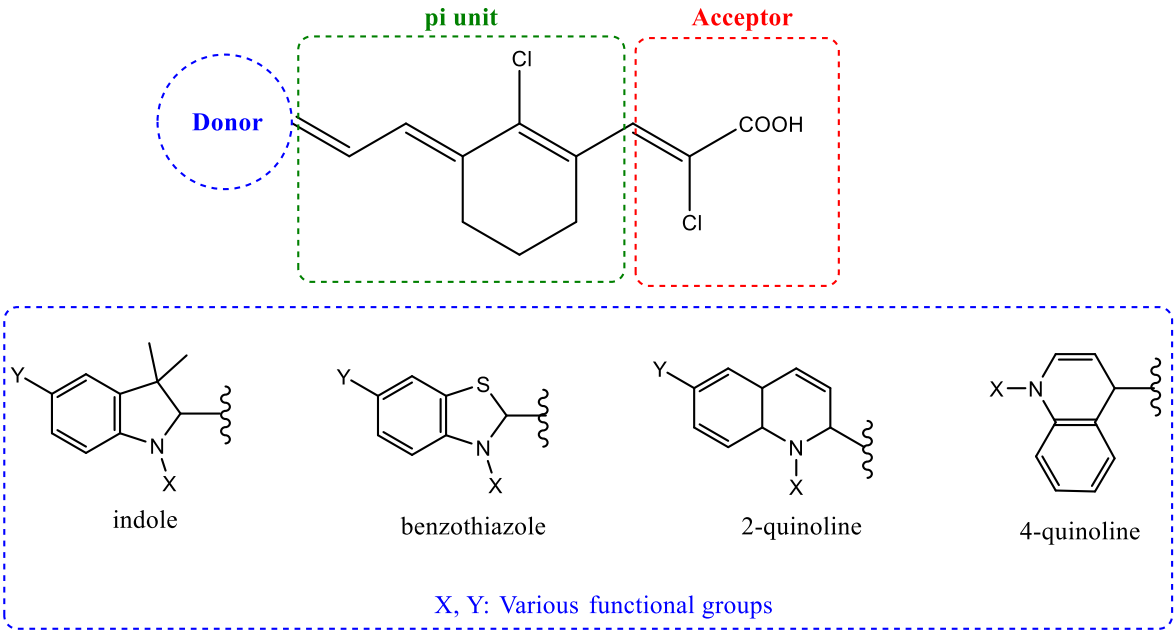

Figure 4: General structure of synthesized D–π-A fluorophores. Refer to the supplementary section for results on benzothiazole, 2-quinolium, and 4-quinolium donor groups.

1.11 Summary and Purpose of Research

In this thesis, DNA interactions and photocleavage of a set of D-π-A fluorophores synthesized by our collaborator professor Maged Henary were investigated. This study included chemical and biological techniques involving plasmid DNA cloning, agarose gel electrophoresis, UV-visible and fluorescence spectroscopies. The dyes under investigation contained a chloroacrylic acid acceptor connected to an indole donor moiety via a π-conjugated linker containing a *meso*-chlorine atom (Figure 1.4). At neutral pH, one set of dyes has a net negative charge of -1 while the second set has a neutral charge. These dyes are being investigated as potential phototherapeutic agents with the aim of reducing the adverse side effects of conventional chemotherapy drugs.

The aims of this research are to investigate the stability of the fluorophores in various solvents and to assess their interactions with DNA. The central focus is to determine the ability of

these dyes to use NIR photons to photocleave DNA. Furthermore, we explored ROS generation to identify the free radicals formed by the dyes during DNA photocleavage reactions as well as to assesses the modes of binding of the dyes to DNA. Chapter 2 focuses on the NIR photocleavage of DNA by four synthesized indole donor group dyes (Figure 1.5). Chapter 3 discusses the experimental methods. Lastly, chapter 4 summarizes findings and discusses future study directions.

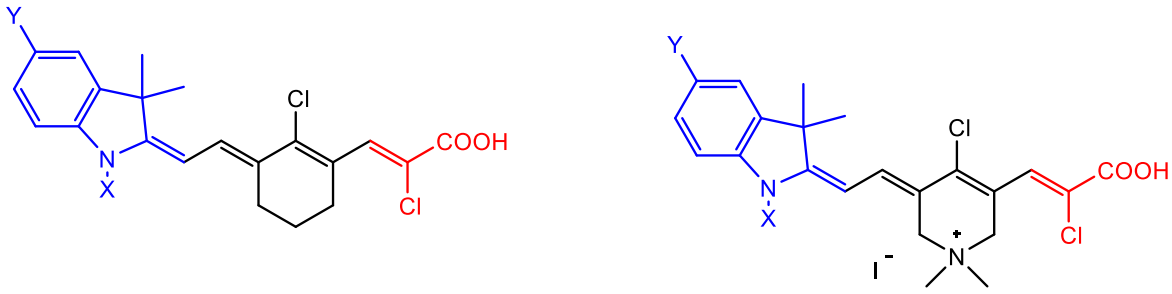

GEO1: X = CH_3 Y = H

GEO32: X = C_2H_5; Y = F

GEO31: X = CH_3 Y = H

GEO30: X = C_2H_5; Y = F

Figure 5: Structures of the indole donor group D–π-A fluorophores under investigation. All dyes were synthesized and provided by Dr. Maged Henary at the Georgia State University, Department of Chemistry.

1.12 References

1. Capella, M. A.; Capella, L. S. A Light in Multidrug Resistance: Photodynamic Treatment of Multidrug-Resistant Tumors. *Journal of Biomedical Science* **2003**, *10* (4), 361–366.
2. Akens, M. K.; Hardisty, M. R.; Wilson, B. C.; Schwock, J.; Whyne, C. M.; Burch, S.; Yee, A. J. Defining the Therapeutic Window of Vertebral Photodynamic Therapy in a Murine Pre-Clinical Model of Breast Cancer Metastasis using the Photosensitizer BPD-MA (Verteporfin). *Breast Cancer Research and Treatment* **2010,** *119* (2), 325-33.
3. Agostinis, P.; Berg, K.; Cengel, K. A.; Foster, T. H.; Girotti, A. W.; Gollnick, S. O.; Hahn, S. M.; Hamblin, M. R.; Juzeniene, A.; Kessel, D.; Korbelik, M.; Moan, J.; Mroz, P.; Nowis, D.; Piette, J.; Wilson, B. C.; Golab, J. Photodynamic Therapy of Cancer: An Update. *A Cancer Journal for Clinicians* **2011,** *61* (4), 250-81.
4. Plotino, G.; Grande, N. M.; Mercade, M. Photodynamic Therapy in Endodontics. *International Endodontic Journal* **2019,** *52* (6), 760-774.
5. Park, Y. K.; Park, C. H. Clinical Efficacy of Photodynamic Therapy. *Obstetrics & Gynecology Science* **2016,** *59* (6), 479-488.
6. Kendall, C. A.; Morton, C. A. Photodynamic Therapy for the Treatment of Skin Disease. *Technology in Cancer Research & Treatment* **2003,** *2* (4), 283-8.
7. Fien, S. M.; Oseroff, A. R. Photodynamic Therapy for Non-Melanoma Skin Cancer. *Journal of the National Comprehensive Cancer Network* **2007,** *5* (5), 531-40.
8. Biel, M. A. Photodynamic Terapy Treatment of Early Oral and Laryngeal Cancers. *Photochemistry and photobiology* **2007,** *83* (5), 1063-8.
9. Dougherty, T. J. An Update on Photodynamic Therapy Applications. *Journal of Clinical Laser Medicine & Surgery* **2002,** *20* (1), 3-7.
10. Zhao, B.; He, Y. Y. Recent Advances in the Prevention and Treatment of Skin Cancer Using Photodynamic Therapy. *Expert Review of Anticancer Therapy* **2010,** *10* (11), 1797-809.
11. Prazmo, E. J.; Kwasny, M.; Lapinski, M.; Mielczarek, A. Photodynamic Therapy As a Promising Method Used in the Treatment of Oral Diseases. *Advances in Clinical and Experimental Medicine* **2016,** *25* (4), 799-807.
12. Mohammadi, Z.; Jafarzadeh, H.; Shalavi, S.; Kinoshita, J. I. Photodvnamic Therapy in Endodontics. *The Journal of Contemporary Dental Practice* **2017,** *18* (6), 534-538.
13. Daniell, M. D.; Hill, J. S. A History of Photodynamic Therapy. *Australian and New Zealand Journal of Surgery* **1991,** *61* (5), 340-8.
14. Møller, K. I.; Kongshoj, B.; Philipsen, P. A.; Thomsen, V. O.; Wulf, H. C. How Finsen's Light Cured Lupus Vulgaris. *Photodermatology, Photoimmunology & Photomedicine* **2005,** *21* (3), 118-24.
15. Hönigsmann, H. History of Phototherapy in Dermatology. *Photochemical and Photobiological Sciences* **2013,** *12* (1), 16-21.
16. Dai, T.; Fuchs, B. B.; Coleman, J. J.; Prates, R. A.; Astrakas, C.; St Denis, T. G.; Ribeiro, M. S.; Mylonakis, E.; Hamblin, M. R.; Tegos, G. P. Concepts and Principles of Photodynamic Therapy as an Alternative Antifungal Discovery Platform. *Frontiers in Microbiology* **2012,** *3*, 120.

17. Spikes, J. D. The Origin and Meaning of the Term “Photodynamic” (as Used in “Photodynamic Therapy”, for Example. *Journal of Photochemistry and Photobiology B: Biology* **1991,** *9* (3), 369-371.
18. Steinbauer, J. M.; Schreml, S.; Kohl, E. A.; Karrer, S.; Landthaler, M.; Szeimies, R. M. Photodynamic Therapy in Dermatology. *Journal of the German Society of Dermatology* **2010,** *8* (6), 454-64.
19. Lee, C. N.; Hsu, R.; Chen, H.; Wong, T. W. Daylight Photodynamic Therapy: An Update. *Molecules* **2020,** *25* (21).
20. Dougherty, T. J.; Gomer, C. J.; Henderson, B. W.; Jori, G.; Kessel, D.; Korbelik, M.; Moan, J.; Peng, Q. Photodynamic Therapy. *Journal of the National Cancer Institute* **1998,** *90* (12), 889-905.
21. Luby, B. M.; Walsh, C. D.; Zheng, G. Advanced Photosensitizer Activation Strategies for Smarter Photodynamic Therapy Beacons. *Angewandte Chemie (International ed. in English)* **2019,** *58* (9), 2558-2569.
22. Issa, M. C.; Manela-Azulay, M. Photodynamic Therapy: A Review of the Literature and Image Documentation. *Anais brasileiros de dermatologia* **2010,** *85* (4), 501-11.
23. Dąbrowski, J. M.; Pucelik, B.; Regiel-Futyra, A.; Brindell, M.; Mazuryk, O.; Kyzioł, A.; Stochel, G.; Macyk, W.; Arnaut, L. G. Engineering of Relevant Photodynamic Processes Through Structural Modifications of Metallotetrapyrrolic Photosensitizers *Coordination Chemistry Reviews.* **2016,** *325*, 67-101.
24. Kim, M. M.; Darafsheh, A. Light Sources and Dosimetry Techniques for Photodynamic Therapy. *Photochemistry and photobiology* **2020,** *96* (2), 280-294.
25. Dąbrowski, J. M.; Arnaut, L. G. Photodynamic Therapy (PDT) of Cancer: From Local to Systemic Treatment. *Photochemical and Photobiological Sciences* **2015,** *14* (10), 1765-80.
26. Smith, A. M.; Mancini, M. C.; Nie, S. Second Window for in Vivo Imaging. *Nature Nanotechnology* **2009,** *4* (11), 710-711.
27. Konopka, K.; Goslinski, T. Photodynamic Therapy in Dentistry. *Journal of Dental Researc.* **2007,** *86* (8), 694-707.
28. Juarranz, A.; Jaén, P.; Sanz-Rodríguez, F.; Cuevas, J.; González, S. Photodynamic Therapy of Cancer. Basic Principles and Applications. *Clinical & Translational Oncology: Official Publication of the Federation of Spanish Oncology Societies and of the National Cancer Institute of Mexico* **2008,** *10* (3), 148-54.
29. Banerjee, S. M.; MacRobert, A. J.; Mosse, C. A.; Periera, B.; Bown, S. G.; Keshtgar, M. R. S. Photodynamic Therapy: Inception to Application in Breast Cancer. *The Breast* **2017,** *31*, 105-113.
30. Van Straten, D.; Mashayekhi, V.; de Bruijn, H. S.; Oliveira, S.; Robinson, D. J. Oncologic Photodynamic Therapy: Basic Principles, Current Clinical Status and Future Directions. *Cancers* **2017,** *9* (2), 19.
31. Celli, J. P.; Spring, B. Q.; Rizvi, I.; Evans, C. L.; Samkoe, K. S.; Verma, S.; Pogue, B. W.; Hasan, T. Imaging and Photodynamic Therapy: Mechanisms, Monitoring, and Optimization. *Chemical Reviews* **2010,** *110* (5), 2795-2838.
32. Abrahamse, H.; Hamblin, M. R. New Photosensitizers for Photodynamic Therapy. *Biochemical Journal* **2016,** *473* (4), 347-64.

33. O'Connor, A. E.; Gallagher, W. M.; Byrne, A. T. Porphyrin and Nonporphyrin Photosensitizers in Oncology: Preclinical and Clinical Advances in Photodynamic Therapy. *Photochemistry and Photobiology* **2009,** *85* (5), 1053-1074.
34. Li, Z.; Grant, K. B. DNA Photo-Cleaving Agents in the Far-Red to near-Infrared Range – A Review. *RSC Advances* **2016,** *6* (29), 24617-24634.
35. Wachowska, M.; Muchowicz, A.; Firczuk, M.; Gabrysiak, M.; Winiarska, M.; Wańczyk, M.; Bojarczuk, K.; Golab, J. Aminolevulinic Acid (ALA) as a Prodrug in Photodynamic Therapy of Cancer. *Molecules* **2011,** *16* (5), 4140-4164.
36. Singh, S.; Nagpal, R.; Manuja, N.; Tyagi, S. P. Photodynamic Therapy: An Adjunct to Conventional Root Canal Disinfection Strategies. *Australian Endodontic Journal: The Journal of the Australian Society of Endodontology Inc* **2015,** *41* (2), 54-71.
37. Brancaleon, L.; Moseley, H. Laser and Non-laser Light Sources for Photodynamic Therapy. *Lasers in Medical Science.* **2002,** *17* (3), 173-86.
38. Ackroyd, R.; Kelty, C.; Brown, N.; Reed, M. The History of Photodetection and Photodynamic Therapy. *Photochemistry and Photobiology* **2001,** *74* (5), 656-69.
39. Wilson, B. C.; Patterson, M. S. The Physics, Biophysics and Technology of Photodynamic Therapy. *Physics in Medicine and Biology* **2008,** *53* (9), R61-109.
40. Breskey, J. D.; Lacey, S. E.; Vesper, B. J.; Paradise, W. A.; Radosevich, J. A.; Colvard, M. D. Photodynamic Therapy: Occupational Hazards and Preventative Recommendations for Clinical Administration by Healthcare Providers. *Photomed Laser Surgery* **2013,** *31* (8), 398-407.
41. Karrer, S.; Szeimies, R. M.; Hohenleutner, U.; Landthaler, M. Role of Lasers and Photodynamic Therapy in the Treatment of Cutaneous Malignancy. *American Journal of Clinical Dermatology* **2001,** *2* (4), 229-37.
42. Landthaler, M.; Szeimies, R. M.; Hohenleutner, U. Laser Therapy of Skin Tumors. *Recent Results in Cancer Research. Fortschritte der Krebsforschung. Progres dans les Recherches sur le Cancer* **1995,** *139*, 417-21.
43. Mang, T. S. Lasers and Light Sources for PDT: Past, Present and Future. *Photodiagnosis Photodynamic Therapy* **2004,** *1* (1), 43-8.
44. Cramer, S. W.; Chen, C. C. Photodynamic Therapy for the Treatment of Glioblastoma. *Frontiers in Surgery* **2019,** *6*, 81.
45. Zhang, Q.; He, J.; Yu, W.; Li, Y.; Liu, Z.; Zhou, B.; Liu, Y. A Promising Anticancer Drug: A Photosensitizer Based on the Porphyrin Skeleton. *RSC Medicinal Chemistry* **2020,** *11* (4), 427-437.
46. Halliwell, B. Free Radicals and Antioxidants - quo vadis? *Trends in Pharmacological Sciences* **2011,** *32* (3), 125-30.
47. Turrens, J. F. Mitochondrial Formation of Reactive Oxygen Species. *Journal of Physiology* **2003,** *552* (Pt 2), 335-344.
48. Grant, J. J.; Loake, G. J. Role of Reactive Oxygen Intermediates and Cognate Redox Signaling in Disease Resistance. *Plant Physiology* **2000,** *124* (1), 21-29.
49. Castano, A. P.; Demidova, T. N.; Hamblin, M. R. Mechanisms in Photodynamic Therapy: Part One-Photosensitizers, Photochemistry and Cellular Localization. *Photodiagnosis and Photodynamic Therapy* **2004,** *1* (4), 279-293.
50. Zepp, R. G.; Faust, B. C.; Hoigne, J. Hydroxyl Radical Formation in Aqueous Reactions (pH 3-8) of Iron(II) with Hydrogen Peroxide: The Photo-Fenton Reaction. *Environmental Science & Technology* **1992,** *26* (2), 313-319.

51. Pospíšil, P.; Prasad, A.; Rác, M. Mechanism of the Formation of Electronically Excited Species by Oxidative Metabolic Processes: Role of Reactive Oxygen Species. *Biomolecules* **2019,** *9* (7).
52. Di Meo, S.; Reed, T. T.; Venditti, P.; Victor, V. M. Role of ROS and RNS Sources in Physiological and Pathological Conditions. *Oxidative Medicine and Cellular Longevity **2016***, 1245049-1245049.
53. Moan, J.; Berg, K. The Photodegradation of Porphyrins in Cells can be used to Estimate the Lifetime of Singlet Oxygen. *Photochemistry and Photobiology* **1991,** *53* (4), 549-53.
54. Gutteridge, J. M.; Halliwell, B. Free Radicals and Antioxidants in the Year 2000. A Historical Look to the Future. *Annals of the New York Academy of Sciences* **2000,** *899*, 136-47.
55. Breen, A. P.; Murphy, J. A. Reactions of Oxyl Radicals with DNA. *Free Radical Biology and Medicine* **1995,** *18* (6), 1033-1077.
56. Dos Santos, A. F.; de Almeida, D. R. Q.; Terra, L. F.; Baptista, M. S.; Labriola, L. Photodynamic Therapy in Cancer Treatment - An Update Review. *Journal of Cancer Metastasis and Treatment* **2019,** *5*, 25.
57. Allison, R. R.; Moghissi, K. Photodynamic Therapy (PDT): PDT Mechanisms. *Clinical Endoscopy* **2013,** *46* (1), 24-29.
58. Reginato, E.; Wolf, P.; Hamblin, M. R. Immune Response After Photodynamic Therapy Increases Anti-Cancer and Anti-Bacterial Effects. *World Journal of Immunology* **2014**, 4 (1), 1-11.
59. Jan, R.; Chaudhry, G.-E. S. Understanding Apoptosis and Apoptotic Pathways Targeted Cancer Therapeutics. *Advanced Pharmaceutical Bulletin* **2019,** *9* (2), 205-218.
60. Allegra, A.; Pioggia, G.; Tonacci, A.; Musolino, C.; Gangemi, S. Oxidative Stress and Photodynamic Therapy of Skin Cancers: Mechanisms, Challenges and Promising Developments. *Antioxidants (Basel, Switzerland)* **2020,** *9* (5).
61. Poon, I. K. H.; Hulett, M. D.; Parish, C. R. Molecular Mechanisms of Late Apoptotic/Necrotic Cell Clearance. *Cell Death & Differentiation* **2010,** *17* (3), 381-397.
62. Wang, X.; Lin, Y. Tumor Necrosis Factor and Cancer, Buddies or Foes? *Acta Pharmaceutica Sinica* **2008,** *29* (11), 1275-1288.
63. Wallach, D.; Varfolomeev, E. E.; Malinin, N. L.; Goltsev, Y. V.; Kovalenko, A. V.; Boldin, M. P. Tumor Necrosis Factor Receptor and Fas Signaling Mechanisms. *Annual Review of Immunology* **1999,** *17*, 331-67.
64. Almeida, R. D.; Manadas, B. J.; Carvalho, A. P.; Duarte, C. B. Intracellular Signaling Mechanisms in Photodynamic Therapy. *Biochimica et Biophysica Acta* **2004,** *1704* (2), 59-86.
65. Oleinick, N. L.; Morris, R. L.; Belichenko, I. The Role of Apoptosis in Response to Photodynamic Therapy: What, Where, Why, and How. *Photochemical & Photobiological Sciences* **2002,** *1* (1), 1-21.
66. Hengartner, M. O. The Biochemistry of Apoptosis. *Nature* **2000,** *407* (6805), 770-776.
67. Collin, F. Chemical Basis of Reactive Oxygen Species Reactivity and Involvement in Neurodegenerative Diseases. *International Journal of Molecular Sciences* **2019,** *20* (10).
68. Auten, R. L.; Davis, J. M. Oxygen Toxicity and Reactive Oxygen Species: The Devil Is in the Details. *Pediatric Research* **2009,** *66* (2), 121-127.
69. Laloi, C.; Havaux, M. Key Players of Singlet Oxygen-Induced Cell Death in Plants. *Frontiers in Plant Science* **2015,** *6*, 39.

70. Pizzino, G.; Irrera, N.; Cucinotta, M.; Pallio, G.; Mannino, F.; Arcoraci, V.; Squadrito, F.; Altavilla, D.; Bitto, A. Oxidative Stress: Harms and Benefits for Human Health. *Oxidative Medicine and Cellular Longevity* **2017,** 8416763-8416763.
71. Gligorovski, S.; Strekowski, R.; Barbati, S.; Vione, D. Environmental Implications of Hydroxyl Radicals (•OH). *Chemical Reviews* **2015,** *115* (24), 13051-13092.
72. Zhou, Z.; Song, J.; Nie, L.; Chen, X. Reactive Oxygen Species Generating Systems Meeting Challenges of Photodynamic Cancer Therapy. *Chemical Society Reviews* **2016,** *45* (23), 6597-6626.
73. Lobo, V.; Patil, A.; Phatak, A.; Chandra, N. Free Radicals, Antioxidants and Functional Foods: Impact on Human Health. *Pharmacognosy Reviews* **2010,** *4* (8), 118-126.
74. Sharma, P.; Jha, A. B.; Dubey, R. S.; Pessarakli, M. Reactive Oxygen Species, Oxidative Damage, and Antioxidative Defense Mechanism in Plants Under Stressful Conditions. *Journal of Botany* **2012,** *2012*, 1-26.
75. Lushchak, V. I. Free Radicals, Reactive Oxygen Species, Oxidative Stress and its Classification. *Chemico- Biological Interactions* **2014,** *224*, 164-75.
76. Forrester Steven, J.; Kikuchi Daniel, S.; Hernandes Marina, S.; Xu, Q.; Griendling Kathy, K. Reactive Oxygen Species in Metabolic and Inflammatory Signaling. *Circulation Research* **2018,** *122* (6), 877-902.
77. Sies, H. Glutathione and its Role in Cellular Functions. *Free Radical Biology & Medicine* **1999,** *27* (9-10), 916-21.
78. Coury, J. E.; McFail-Isom, L.; Williams, L. D.; Bottomley, L. A. A Novel Assay for Drug-DNA Binding Mode, Affinity, and Exclusion Number: Scanning Force Microscopy. *Proceedings of the National Academy of Sciences of the United States of America* **1996,** *93* (22), 12283-6.
79. Sischka, A.; Toensing, K.; Eckel, R.; Wilking, S. D.; Sewald, N.; Ros, R.; Anselmetti, D. Molecular Mechanisms and Kinetics between DNA and DNA Binding Ligands. *Biophysical Journal* **2005,** *88* (1), 404-11.
80. Aleksić, M. M.; Kapetanović, V. An Overview of the Optical and Electrochemical Methods for Detection of DNA - Drug Interactions. *Acta chimica Slovenica* **2014,** *61* (3), 555-73.
81. Becker, H. C.; Norden, B. DNA Binding Mode and Sequence Specificity of Piperazinylcarbonyloxyethyl Derivatives of Anthracene and Pyrene. *Journal of American Chemical Society* **1999,** *121* (51), 11947-11952.
82. Armitage, B. A.. Cyanine Dye-DNA Interactions: Intercalation, Groove Binding, and Aggregation. In *DNA Binders and Related Subjects* **2005**; pp 55-76.
83. Ogulchansky, T. Y.; Losytskyy, M. Y.; Kovalska, V. B.; Lukashov, S. S.; Yashchuk, V. M.; Yarmoluk, S. M. Interaction of Cyanine Dyes with Nucleic Acids. XVIII. Formation of the Carbocyanine Dye J-aggregates in Nucleic Aacid Grooves. *Spectrochimica Acta Part A: Molecular and Biomolecular Spectroscopy* **2001,** *57* (13), 2705-15.
84. Kellett, A.; Molphy, Z.; Slator, C.; McKee, V.; Farrell, N. P. Molecular Methods for Assessment of Non-covalent Metallodrug-DNA Interactions. *Chemical Society Reviews* **2019,** *48* (4), 971-988.
85. Phadte, A. A.; Banerjee, S.; Mate, N. A.; Banerjee, A. Spectroscopic and Viscometric Determination of DNA-Bnding Modes of some Bioactive Dibenzodioxins and Phenazines. *Biochemistry and Biophysics Reports* **2019,** *18*, 100629.

86. Palchaudhuri, R.; Hergenrother, P. J. DNA As a Target for Anticancer Compounds: Methods to Determine the Mode of Binding and the Mmechanism of Action. *Current Opinion in Biotechnology* **2007,** *18* (6), 497-503.
87. De Almeida, S. M. V.; Ribeiro, A. G.; de Lima Silva, G. C.; Ferreira Alves, J. E.; Beltrão, E. I. C.; de Oliveira, J. F.; de Carvalho, L. B. J.; Alves de Lima, M. D. C. DNA Binding and Topoisomerase Inhibition: How Can These Mechanisms be Explored to Design More Specific Anticancer Agents? *Biomedicine & Pharmacotherapy* **2017,** *96*, 1538-1556.
88. Armitage, B. Photocleavage of Nucleic Acids. *Chemical Reviews* **1998,** *98* (3), 1171-1200.
89. Da Ros, T.; Spalluto, G.; Boutorine, A. S.; Bensasson, R. V.; Prato, M. DNA-Photocleavage Agents. *Current Pharmaceutical Design* **2001,** *7* (17), 1781-821.
90. Li, Z. Y.; Grant, K. B. DNA Photo-Cleaving Agents in the Far-Red to Near-Infrared Range - A Review. *Rsc Advances* **2016,** *6* (29), 24617-24634.
91. Chadalavada, D. M.; Bevilacqua, P. C. Analyzing RNA and DNA Folding using Temperature Gradient Gel Electrophoresis (TGGE) with Application to in Vitro Selections. *Methods in Enzymology* **2009,** *468*, 389-408.
92. Lee, P. Y.; Costumbrado, J.; Hsu, C. Y.; Kim, Y. H. Agarose Gel Electrophoresis for the Separation of DNA Fragments. *Journal of Visualized Experiments* **2012,** (62).
93. Vieira, J.; Messing, J. The pUC Plasmids, an M13mp7-Derived System for Insertion Mutagenesis and Sequencing with Synthetic Universal Primers. *Gene* **1982,** *19* (3), 259-68.
94. Yanisch-Perron, C.; Vieira, J.; Messing, J. Improved M13 Phage Cloning Vectors and Host Strains: Nucleotide Sequences of the M13mpl8 and pUC19 Vectors. *Gene* **1985,** *33* (1), 103-119.
95. Feliciello, I.; Chinali, G. A Modified Alkaline Lysis Method for the Preparation of Highly Purified Plasmid DNA from Escherichia coli. *Analytical Biochemistry* **1993,** *212* (2), 394-401.
96. Bindu, P. J.; Mahadevan, K. M.; Satyanarayan, N. D.; Ravikumar Naik, T. R. Synthesis and DNA Cleavage Studies of Novel Quinoline Oxime Esters. *Bioorganic & Medicinal Chemistry Letters* **2012,** *22* (2), 898-900.
97. Monro, S.; Colón, K. L.; Yin, H.; Roque, J., 3rd; Konda, P.; Gujar, S.; Thummel, R. P.; Lilge, L.; Cameron, C. G.; McFarland, S. A. Transition Metal Complexes and Photodynamic Therapy from a Tumor-Centered Approach: Challenges, Opportunities, and Highlights from the Development of TLD1433. *Chemical Reviews* **2019,** *119* (2), 797-828.
98. Rémond, M.; Zheng, Z.; Jeanneau, E.; Andraud, C.; Bretonnière, Y.; Redon, S. 4,5,5-Trimethyl-2,5-Dihydrofuran-Based Electron-Withdrawing Groups for Nir-Emitting Push–Pull Dipolar Fluorophores. *The Journal of Organic Chemistry* **2019**, *84* (16), 9965–9974.
99. Owens, E. A.; Henary, M.; El Fakhri, G.; Choi, H. S. Tissue-Specific near-Infrared Fluorescence Imaging. *Accounts of Chemical Research* **2016**, *49* (9), 1731–1740.
100. Yang, J.; Ganesan, P.; Teuscher, J.; Moehl, T.; Kim, Y.; Yi, C.; Comte, P.; Pei, K.; Holcombe, T.; Nazeeruddin, M.; Hua, J.; Zakeeruddin, S.; Tian, H.; Grätzel, M. Influence of the Donor Size in D–π–A Organic Dyes for DyeSensitized Solar Cells. *Journal of American Chemical Society* **2014**, 136(15), 5722–5730.

101. Zhao, B.; Xie, G.; Wang, H.; Han, C.; Xu, H. Simply Structured near-Infrared Emitters with a Multicyano Linear Acceptor for Solution-Processed Organic Light-Emitting Diodes. *Chemistry - A European Journal* **2019**, *25* (4), 895–895.
102. Zhang, Q.; Zhang, J.; Zuo, H.; Wang, C.; and Shen, Y. A Novel Colorimetric and Fluorescent Sensor for Cyanide Anions Detection Based on Triphenylamine and Benzothiadiazole. *Tetrahedron* **2016**, 72(9), 1244–1248.
103. Cvejn, D.; Achelle, S.; Pytela, O.; Malval, J.-P.; Spangenberg, A.; Cabon, N.; Bureš, F.; Robin-le Guen, F. Tripodal Molecules with Triphenylamine Core, Diazine Peripheral Groups and Extended π-Conjugated Linkers. *Dyes and Pigments* **2016**, *124*, 101–109.

2 DNA PHOTOCLEAVAGE BY NIR INDOLE DONOR GROUP FLUOROPHORES

2.1 Abstract

Herein, we report the synthesis of and DNA photocleavage by four D–π-A fluorophores with a chloroacrylic acid acceptor linked to an indole donor group via a π-conjugated linker incorporating a cyclohexene and a *meso*-chlorine atom. Dyes **GEO30**, **GEO32**, **GEO31**, and **GEO1** were unstable in aqueous buffer, but exhibited DNA-dye interaction. UV–visible spectra suggested that the neutral dyes **GEO30** and **GEO31** bind at high DNA concentrations. As the ratio of DNA to dye is increased, an apparent aggregate is converted to a putative monomeric dye form of **GEO30** and **GEO31.** Competitive binding studies suggest that **GEO30** and **GEO31** interact with the minor and major grooves of DNA. Both dyes were relatively unreactive in the dark, but under 750 nm irradiation, they generated hydroxyl radicals that cleaved DNA in high yields. The fluorinated dye **GEO30** exhibited the most DNA cleavage.

2.2 Introduction

For the D–π-A fluorophores, the linker unit was synthesized by the Henary's group via the Vilsmeier Haack reaction procedure. First, cyclohexanone (**1**) was reacted with dichloromethane (DCM), and phosphoryl chloride ($POCl_3$) in *N*, *N*-dimethylformamide (DMF) to yield carbaldehyde (2) (Figure 2.1).[1] Then, under basic conditions, the chloroacrylic acid, which serves as both an acceptor and linker, was prepared by reacting carbaldehyde (**2**) with chloroacetic acid. Subsequently, indolium, 2- quinolinium, and 4- quinolinium heterocyclic salts were reacted with the linker and acceptor unit (**3**) in ethanol under basic conditions to generate the desired D–π-A fluorophores (**GEO30** and **GEO31**). **GEO32** and **GEO1** were the set of dyes that have a net negative charge of -1 while **GEO30** and **GEO31** are zwitterionic (Figure 1.4). The syntheses of the zwitterionic compounds cannot be mentioned as they have yet to be

published.

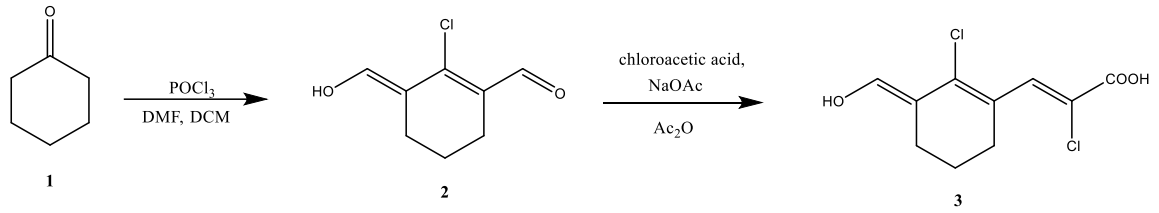

Figure 6: Synthesis of chloroacrylic acid acceptor and π linker units.[1]

The electron acceptor carboxylic acid, combined with the inductively withdrawing effect of chloride, results in a strong electron acceptor group for all four dyes. A push-pull mechanism is created by the combination of electron donor and acceptor units, resulting in fluorophores with absorption in the NIR window. Depending on the shape and properties of the fluorophores, they could have the ability to form stable complexes with dsDNA in monomeric and/or aggregated forms. Fluorophores can bind to DNA through intercalation, groove binding, and/or external electrostatic interactions, depending on the structure and aggregation state of the dye.[2-5] The factors that influence the optical properties of D–π-A fluorophores are the strength of donor and acceptor groups, the nature and length of the linker unit, and planarization of the molecules.[1] Alternating between the indole, benzothiazole, and quinoline donor heterocyclic rings have been reported to affect the absorption coefficients, fluorescence quantum yields, and absorption and emission maxima of fluorophores.[1] The fluorophores exhibited high absorption in the NIR (700-970 nm) range due to the improved intramolecular charge transfer (ICT) between the donor moieties and chloroacrylic acid linked by the Vilsmeier-Haack linker.

In photodynamic therapy (PDT), a photosensitizer (PS) is activated in diseased tissues using a light source. Due to deep penetration through biological tissue, a light source with a NIR wavelength between 700 nm to 900 nm is ideal for biological applications.[6] Through the interaction of the triplet excited state (^{3}PS*) of the photosensitizer and the ground state triplet

oxygen ($^3O_2$), highly localized, short-lived ROS are produced.[7-9] Two significant ROS are produced via Type 1 or Type 2 reaction mechanisms. In Type 1 electron transfer, superoxide anion radicals ($O_2^{\bullet-}$) produce highly reactive hydroxyl radicals (•OH) via an H_2O_2 intermediate, whereas singlet oxygen ($^1O_2$) is produced via Type 2 energy transfer.[10, 11] In irradiated cells, $^1O_2$ and OH° are highly localized, causing oxidative damage to DNA and other macromolecules at diffusion distances of 50–100 [24] and 0.8–6.0 nm [25], respectively.[12] This precise localization enhances clinical outcomes in the treatment of diseases, such as cancer due to reduced side effects.[13]

Here, we report the photo-stability, optical properties, and DNA photocleavage activities of four asymmetrical donor acceptor fluorophores (**GEO30**, **GEO32**, **GEO31**, and **GEO1**) containing an indole donor moiety. Shown in the Supplementary Information section, we also investigated the photo-stability and DNA cleavage of three additional fluorophores: **14**, **19**, and **20** with a benzothiazole, 2-quinolium, and 4-quinolium donor group, respectively. We employed HPF fluorescent probe and chemical additives to determine the type of ROS generated and UV-visible spectrophotometry to ascertain the binding mode of dyes **GEO30** and **GEO31** to DNA.

2.3 Results and Discussion

2.3.1 UV-visible Spectrophotometry: Dye Stability and DNA-dye Interactions

In the first set of experiments, UV–visible spectroscopic spectra of the dyes were examined in various media and recorded as a function of time to investigate the photo-stability of the fluorophores. Photo-stability studies are very important in determining the photophysical properties of fluorophores. In solution, the dyes can undergo autooxidation as well as oxidative photodegradation known as photobleaching, where the dyes absorb ambient light and lose their fluorescence abilities. Factors that can affect the photostability and aggregation of the dyes are the solvents and donor moiety, which can be functionalized with various groups.

The UV-visible time course absorption spectra were recorded with 10 µM of dyes **GEO30**, **GEO32**, **GEO31**, or **GEO1** in 10 mM of sodium phosphate buffer (pH = 7.0) in the presence and absence of 150 µM bp calf thymus (CT) DNA, and in DMSO at time intervals up to 30 min at 22 °C. Dye **GEO30** is a fluorinated indole containing fluorophore with an ethyl functionalized nitrogen atom and a neutral net charge. The dye was unstable in aqueous buffer losing absorption over time with a λ_{max} value at 743 nm (Figure 2.2A). It exhibited DNA interaction with a λ_{max} shift of the putative monomer to 753 nm (Figure 2.2E). Binding to DNA also substantially stabilized the dye. In DMSO, the dye has λ_{max} values at 763 nm and 459 nm, which shift from 763 nm to 459 nm over time indicative that the dye changes aggregation or decomposes in solution, thus disrupting the 763 nm peak (Figure 2.2I). Dye **GEO32** was also unstable in aqueous buffer with a λ_{max} value at 737 nm (Figure 2.2B). The dye was stabilized by DNA forming λ_{max} values at 705 nm, 765 nm, and 820 nm (Figure 2.2F). In DMSO, the dye forms a putative, relatively stable monomeric peak with a λ_{max} value at 795 nm (Figure 2.2J). Dye **GEO31** is an indole containing fluorophore with a methyl functionalized nitrogen atom and a neutral net charge. In aqueous buffer, the dye exhibited a λ_{max} value at 737 nm. The absorbance decreased over time, showing that the dye is unstable (Figure 2.2C) The addition of DNA increased the absorption signal and formed a stable putative monomer form of the dye with a λ_{max} value at 748 nm (Figure 2.2G). In DMSO, the dye had λ_{max} values at 758 nm and 446 nm, which suggests that the dye changes aggregation or is decomposing over time (Figure 2.2K). Dye **GEO1**, with a λ_{max} value at 771 nm, demonstrated low stability in aqueous buffer (Figure 2.2D). In the presence of DNA, the dye exhibited DNA interactions because the λ_{max} value shifted slowly over time to 783 nm (Figure 2.2H). It was observed that the absorbance at 782 nm decreased up to 5 min and then increased gradually up to

30-min time, suggesting that the dye is switching from free to DNA bound. In DMSO, the dye was stable with a putative monomeric peak appearing at a λ_{max} value of 791 nm (Figure 2.2L).

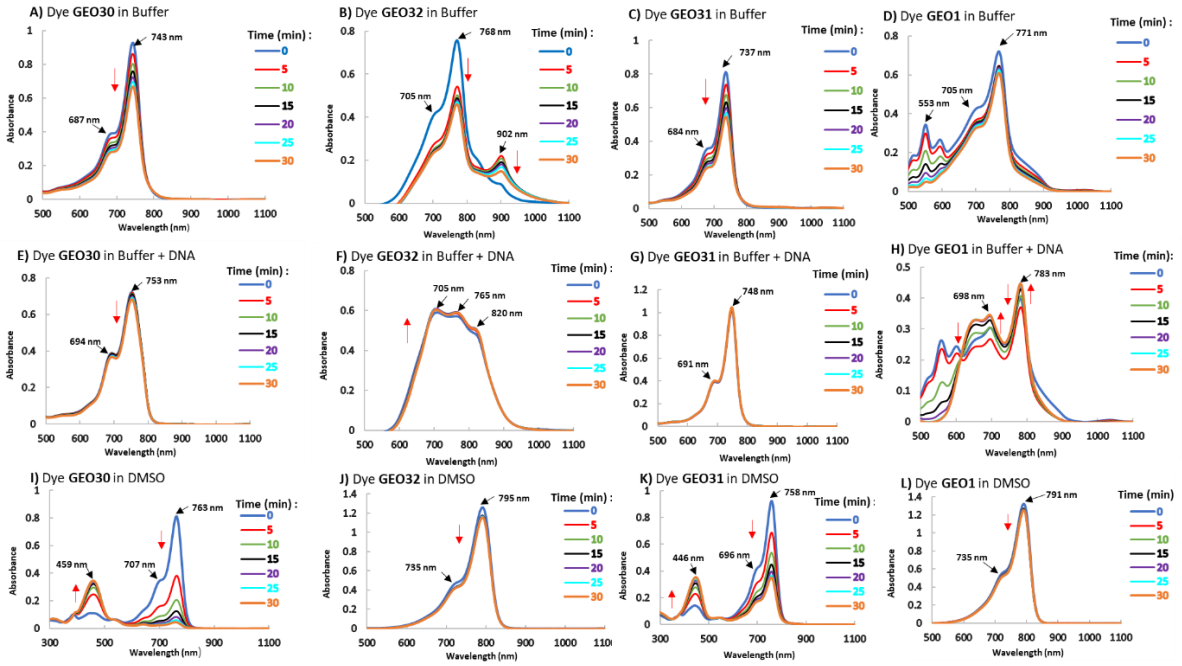

*Figure 7: UV–visible time course spectra recorded for 30 min (22 °C) using 10 µM of dyes **GEO30**, **GEO32**, **GEO31**, and **GEO1**: in the absence (A, B, C, D) and in the presence (E, F, G, H) of 150 µM bp CT DNA, 10 mM sodium phosphate buffer pH =7; and in DMSO (I, J, K, L).*

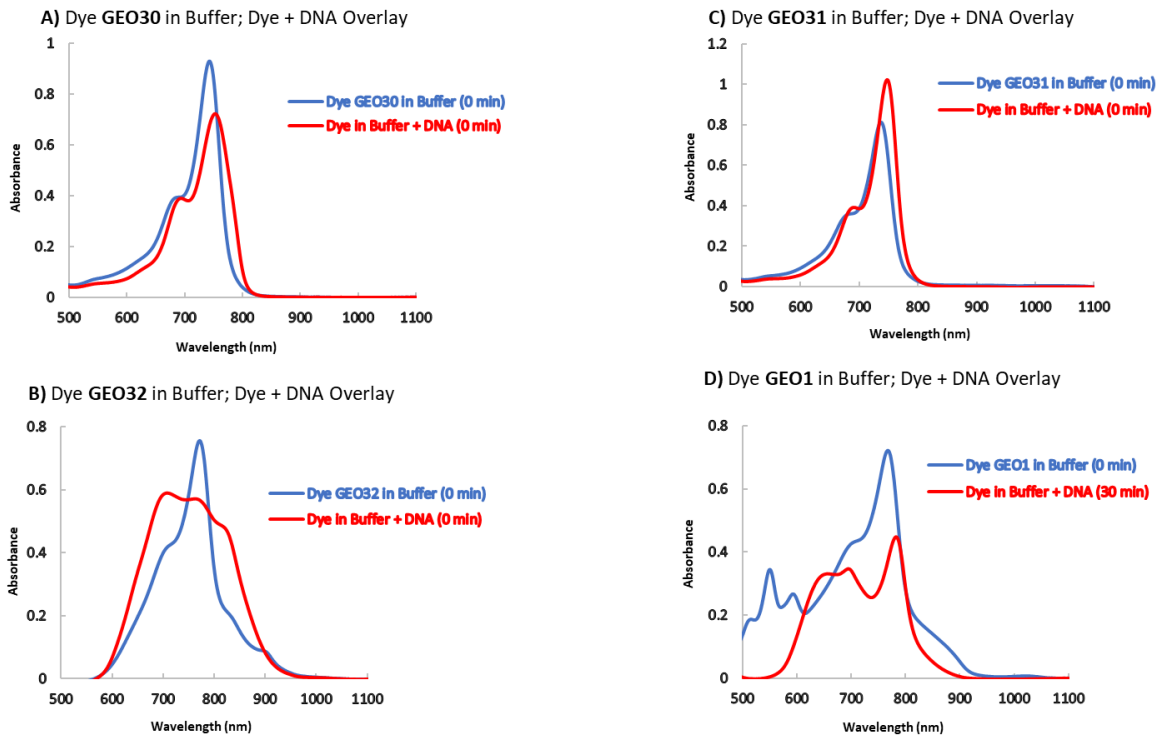

*Figure 8: UV-visible overlay spectra at 0 min or 30 min for 10 µM of dyes **GEO30**, **GEO32**, **GEO31**, and **GEO1** in 10 mM sodium phosphate buffer pH 7.0 in the absence and presence of 150 µM CT DNA (22 °C) with: (A) is an overlaid spectra of 2.2A,E; (B) is an overlaid spectra of 2.2A, E; (B) is an overlaid spectra of 2.2B, F; (C) is an overlaid spectra of 2.2C, G; and (D) is an overlaid spectra of 2.2D, H.*

The overlay spectra further demonstrated that dyes **GEO30**, **GEO32**, **GEO31**, and **GEO1** exhibited DNA interactions. In the presence of DNA, it is observed that **GEO30** becomes red shifted (bathochromic) with putative monomer absorption at 753 nm (Figure 2.3A). For **GEO32**, DNA stabilized the dye possibly forming aggregates in solution (Figure 2.3B). The addition of DNA caused a bathochromic shift of **GEO31** with an absorption value at 748 nm (Figure 2.3C). For **GEO1** the 30-minute time point was used in the overlaid spectrum because the dye became bound to DNA slowly. It exhibited DNA interactions with a bathochromic shift to 783 nm (Figure 2.3D).

2.3.2 DNA Photocleavage at 780 nm

The goal in this study was to investigate the photo-nuclease activity of fluorophores **GEO30**, **GEO32**, **GEO31**, and **GEO1** under physiological conditions. In the aim of finding new phototherapeutic agents, near-infrared 780-nm LED laser was utilized. This wavelength of light was chosen due to its output overlapping with the DNA-bound dye absorption spectra in Figure 2.2E, F, G, H. The reaction solutions contained 10 mM sodium phosphate buffer pH 7.0, 38 μM bp pUC19 plasmid DNA, 0-70 μM of dyes **GEO30**, **GEO32**, **GEO31**, and **GEO1**. The reactions were immersed in an ice bath and either left in the dark or irradiated for 30 min with a 780 nm LED laser. After the 30 min of irradiation, the samples were subjected to electrophoresis on a non-denaturing 1.5 % agarose gel for 60 min.

Dyes **GEO30** and **GEO31** exhibited DNA photocleavage at high dye concentrations (Figure 2.4B and 2.5B). In contrast, **GEO32** and **GEO1** showed low DNA cleavage across the various dye concentrations employed (Figure 2.4D and 2.5D). Fluorinated **GEO30** cleaved DNA better than the other three dyes with an optimal cleavage at 40 μM of dye. Due to the low photocleavage yields of **GEO32** and **GEO1,** (which have a negative net charge at pH 7) these compounds were not studied further, and additional analyses were done on the neutral zwitterionic dyes, **GEO30** and **GEO31**.

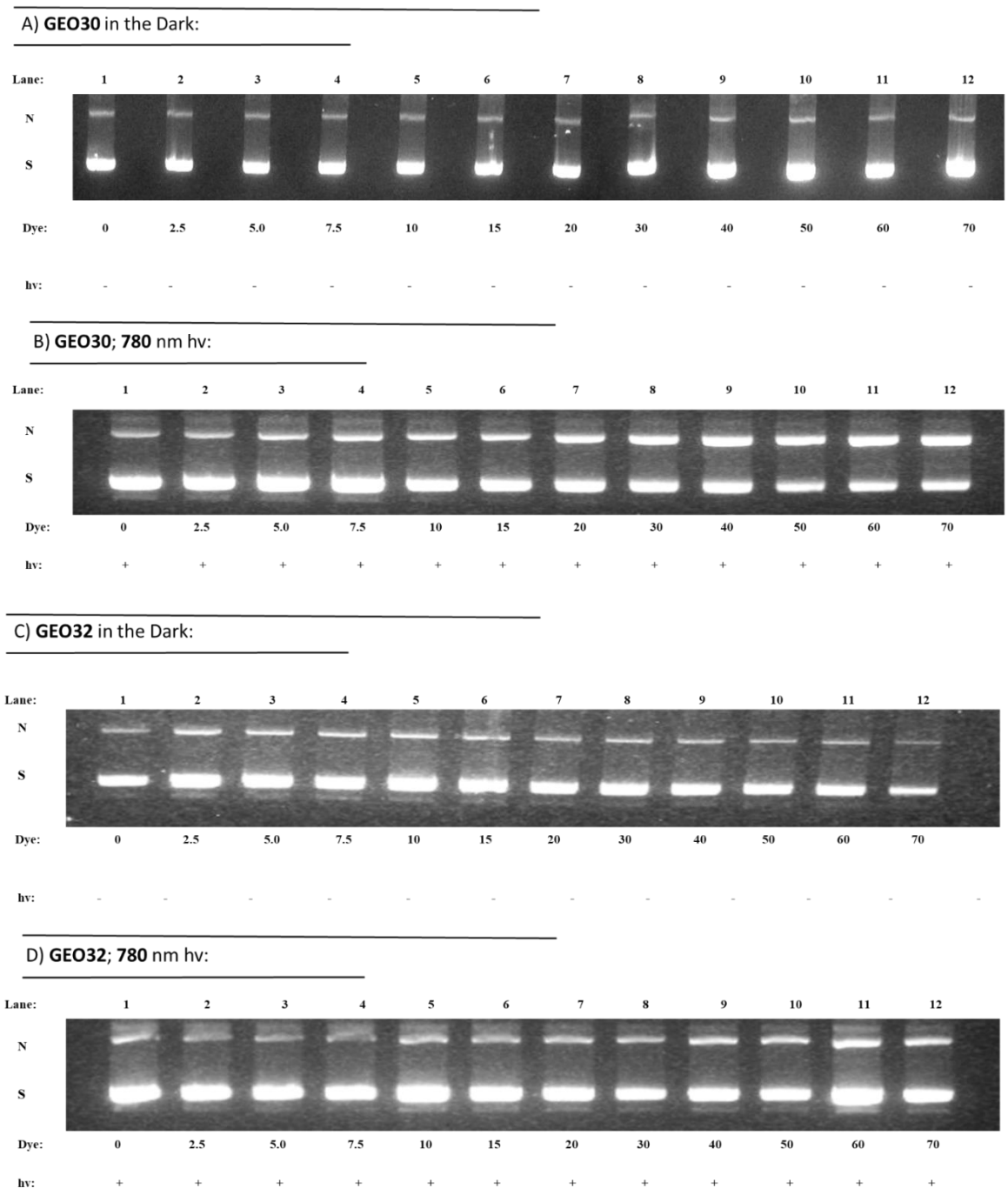

Figure 9: Representative dye-sensitized photocleavage reaction products of pUC19 plasmid DNA by dyes: (A, B) ***GEO30****, and (C, D)* ***GEO31*** *resolved on 1.5 % agarose gel. Reactions contained 10 mM sodium phosphate buffer pH 7.0, 38 µM bp pUC19 plasmid DNA in the absence and presence of 0-70* µM dye. *Each reaction was either kept in the dark or irradiated for 30 min with a* 780 nm LED *laser. A metal block was used to hold the samples and was emersed in an ice bath during the reaction. Abbreviations: N, nicked; S, supercoiled.*

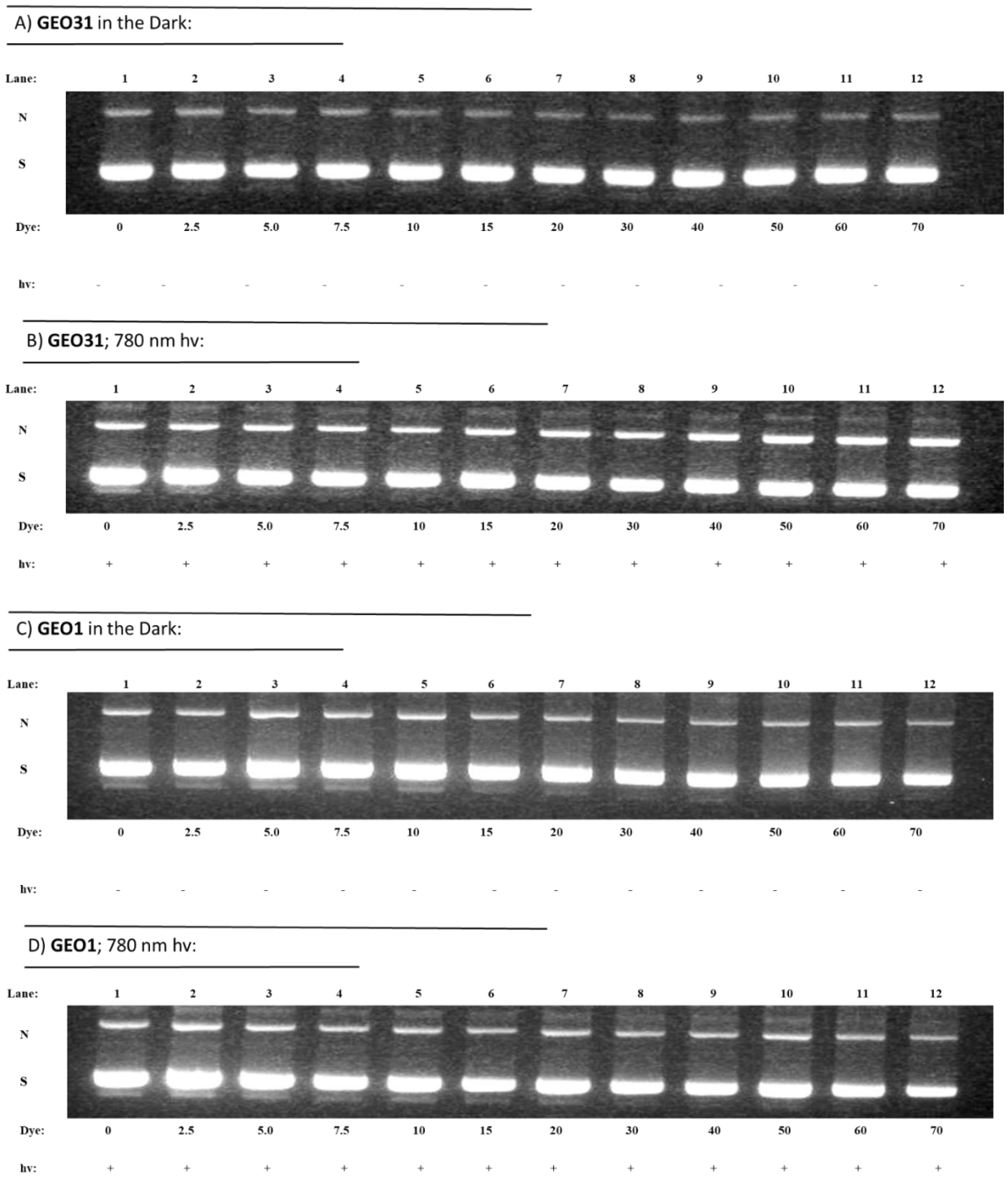

Figure 10: Representative dye-sensitized photocleavage reaction products of pUC19 plasmid DNA by dyes: (A, B) GEO31, and (C, D) GEO1 resolved on 1.5 % agarose gel. Reactions contained 10 mM sodium phosphate buffer pH 7.0, 38 μM bp pUC19 plasmid DNA in the absence and presence of 0-70 μM dye. Each reaction was either kept in the dark or irradiated for 30 min with a 780 nm LED laser. A metal block was used to hold the samples and was emersed in an ice bath during the reaction. Abbreviations: N, nicked; S, supercoiled.

2.3.3 DNA Photocleavage at 750 nm

GEO30 and **GEO31** were further investigated using a 750 nm LED medical lamp. It was observed that for both dyes, as the concentration of dye increased in the light reactions, the photocleavage yield increased substantially compared to the dark control reactions. This is evident because there was a significant increase of nicked DNA at higher concentrations of the dyes (Figure 2.6B, D). The dark reaction, which were the controls exhibited lower levels of photocleavage as expected. Additionally, fluorinated GEO30 cleaved DNA a greater extent than GEO31. Furthermore, placing the reactions in a metal block immersed in an ice bath during photocleavage reactions are not likely to be thermally driven. Rather, **GEO30** and **GEO31** are photochemically cleaving DNA. Optimal DNA cleavage was achieved at 40 μM of dye for **GEO30** and **GEO31**.

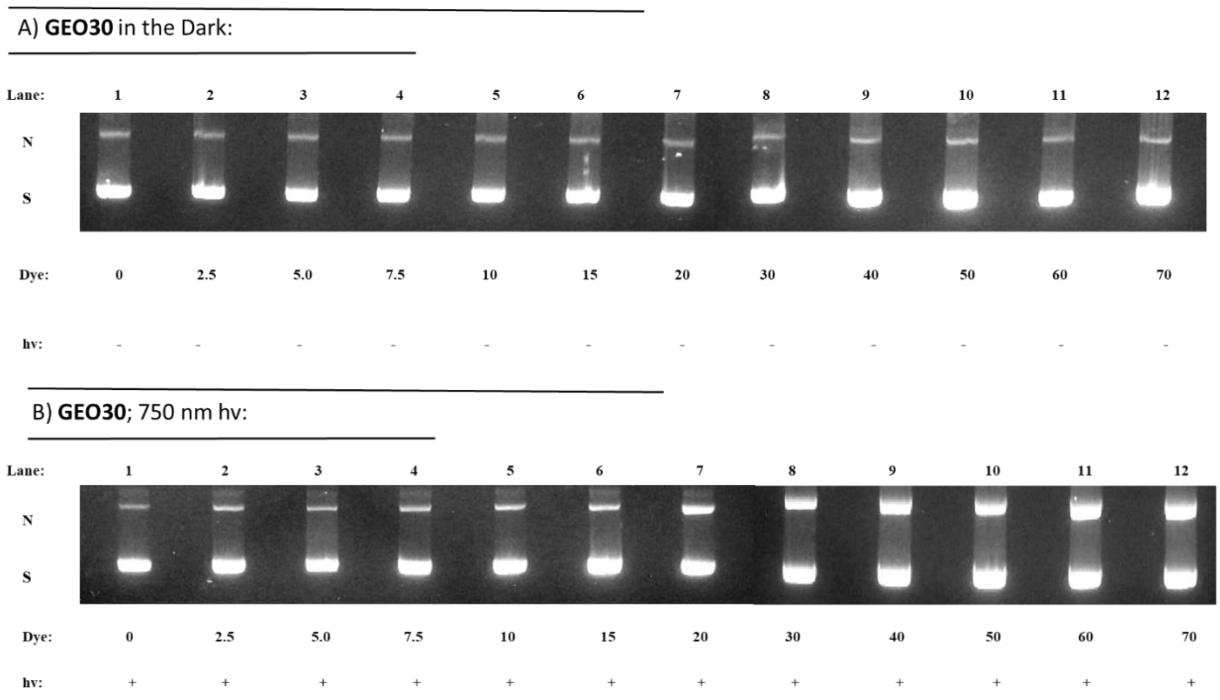

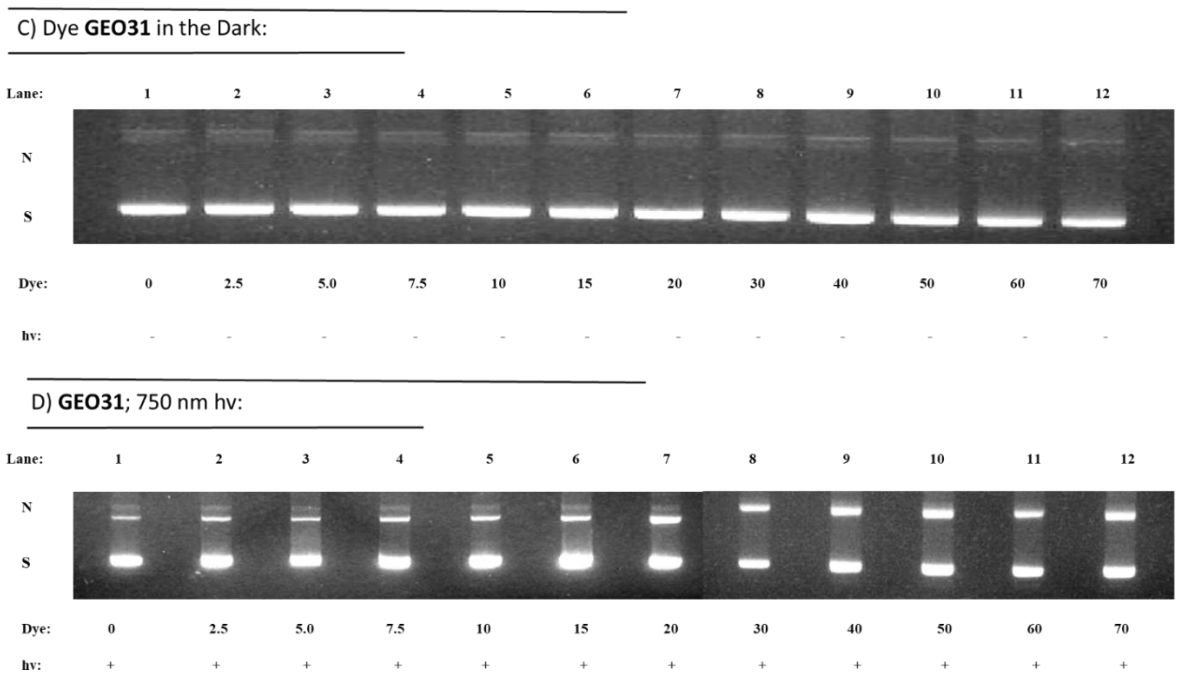

Figure 11: Representative dye-sensitized photocleavage reaction products of pUC19 plasmid DNA by dyes: (A, B) ***GEO30****, and (C, D)* ***GEO31*** *resolved on 1.5 % agarose gels. Reactions contained 10 mM sodium phosphate buffer pH 7.0, 38 µM bp pUC19 plasmid DNA in the absence and presence of 0-70 µM dye. Each reaction was either kept in the dark or irradiated for 30 min with a 750 nm LED medical lamp. A metal block was used to hold the samples and was emersed in an ice bath during the reaction. Abbreviations: N, nicked; S, supercoiled.*

2.3.4 Investigation of DNA Interaction by UV-visible and Fluorescence Spectrophotometric Analyses

In this part of the study, the interaction between dyes **GEO30** and **GEO31** with DNA were investigated. The UV-visible absorption spectra of the dyes were recorded upon the sequential addition of small amounts of calf thymus DNA (CT DNA) titrant to a sample containing 10 µM of dye **GEO30** or **GEO31** in 10 mM sodium phosphate (pH = 7.0) at 22 °C (initial volume 500 µL). These spectrophotometric analyses were conducted to help ascertain the binding modes and to better understand how dye aggregation might affect DNA interactions.

It has been reported for cyanine dyes that increasing the amount of CT DNA disrupts dye aggregation patterns to favor the DNA bound monomers.[14-17] The dye's absorption spectra are

often employed to examine these variations in aggregation state. In the absence of DNA dye **GEO30** showed an absorption λ_{max} value at 742 nm. The sequential addition of 33 and 67 µM bp of DNA decreased the absorption signal at the 745 nm λ_{max} value. Then, from 134 to 1539 µM bp of DNA, the absorption signal increased and shifted the λ_{max} value to 748 nm (Figure 2.7A). This was indicative of the dye gradually switching from free to the DNA-bound dye form. An endpoint in the DNA titration was not reached to the maximum concentration of DNA added. For **GEO31**, a λ_{max} value at 739 nm is seen in the absence of DNA. The introduction of 33 µM bp of DNA, it was observed that the dye in a partially DNA bound state due to the decreased absorption value with a λ_{max} at 746 nm (Figure 2.7B). Then, from 67 to 1539 µM bp of DNA, the data show increased DNA binding because the absorption signal increased in intensity shifting the λ_{max} value to 749 nm. The endpoint was reached at 1078 µM bp of DNA. The appearance of the spectra of DNA bound dye in Figure 2.7 are similar in appearance of the spectra of DNA-bound monomeric cyanine.[22]

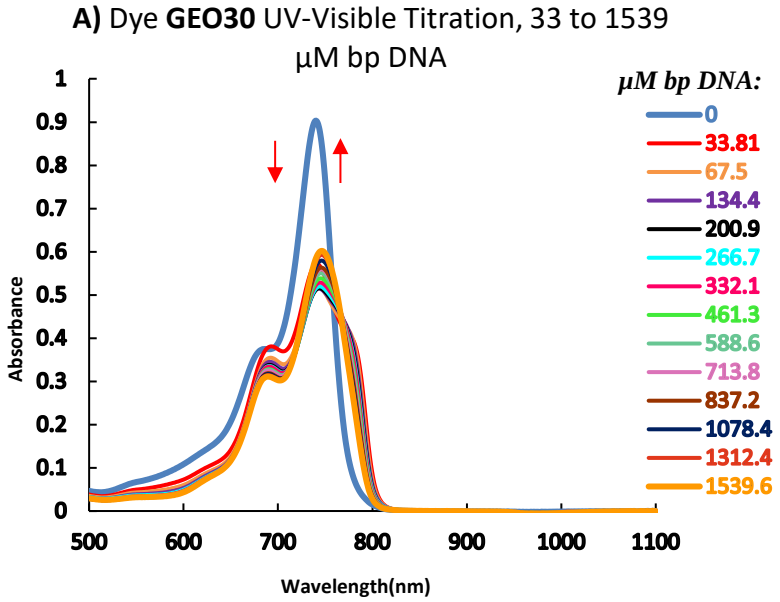

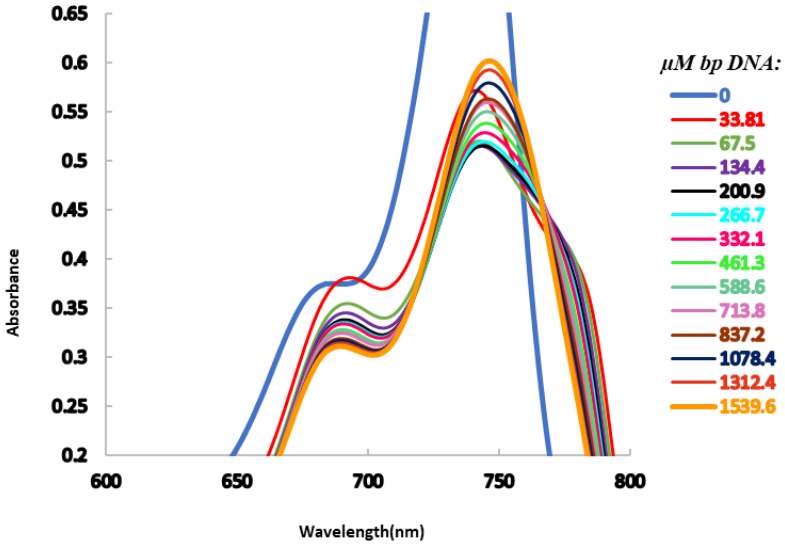

B) Dye **GEO31** UV-Visible Titration, 33 to 1539 µM bp DNA

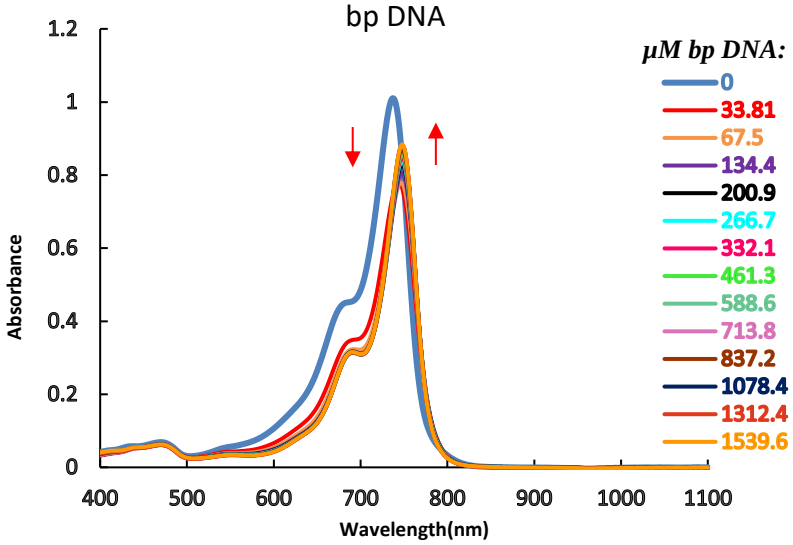

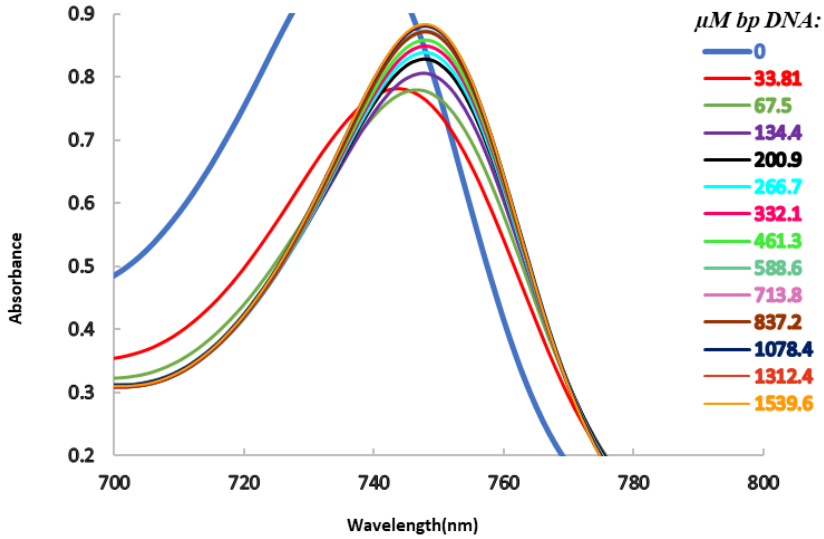

Figure 12: UV–visible absorption titration spectra of dye: (A) ***GEO30*** *and (B)* ***GEO31****. Samples contained 10 µM dye, 10 mM sodium phosphate buffer (pH = 7.0) in the absence and presence of increasing CT DNA concentrations from 31 up to 1409 µM bp. All absorption spectra and DNA concentrations were adjusted for sample dilution (22 °C).*

To further assess the way that dyes **GEO30** and **GEO31** interact with DNA, fluorescence spectrophotometry was utilized. The fluorescence spectra were recorded with 10 µM of dye **GEO30** or **GEO31** in 10 mM sodium phosphate buffer (pH = 7.0) in the absence and presence of increasing CT DNA concentration ranging from 134 to 1312 µM bp (Figure 2.8, 2.9). Reactions containing dye **GEO30** or **GEO31** in the absence of DNA were excited with two distinct excitation wavelengths (λ_{ex} = 740 and 750 nm) to target the maximal absorptions of the free dye. In the presence of DNA, the samples containing **GEO30** or **GEO31** were excited with two wavelengths (λ_{ex} = 740 and 750 nm) to target the DNA-dye complex. For **GEO30**, at excitation wavelengths of 740 and 750 nm in the absence of DNA, emission wavelengths are seen at 743 and 755 nm (134, 588, 1078 and 1312 µM bp DNA). At excitation wavelengths of 740 and 750 nm in the presence of DNA, emission wavelengths appear at 746 and 756 nm (134 and 588 µM bp DNA), and 745

and 756 nm (1078 and 1312 µM bp DNA). For **GEO31**, at excitation wavelengths of 740 and 750 nm in the absence of DNA, emission wavelengths are observed at 745 and 751 nm (134, 588, 1078, and 1312 µM bp DNA). At excitation wavelengths of 740 and 750 nm in the presence of DNA, emission wavelengths appear at 745 and 756 nm (134, 588, 1078, and 1312 µM bp DNA).

A molecule can experience either fluorescence or light scattering when irradiated at specific wavelengths. The difference between light scattering and fluorescence is that fluorescence is a long-lived electronic state phenomenon while light scattering is short-lived. A fluorescent molecule usually has a Stokes shift of at least 10 nm higher than its excitation wavelength.[23] Notwithstanding the fact that the emission of DNA bound **GEO30** is red shifted with respect to the free **GEO30** when excited at 740 nm suggests a contribution from fluorescence. This is not the case under 750 nm excitation suggesting light scattering is the major effect. In the case of **GEO31**, light scattering is indicated at 740 and at 750 nm excitation due to the emission of free and DNA bound **GEO31** being less than 10 nm from the excitation wavelength**.**

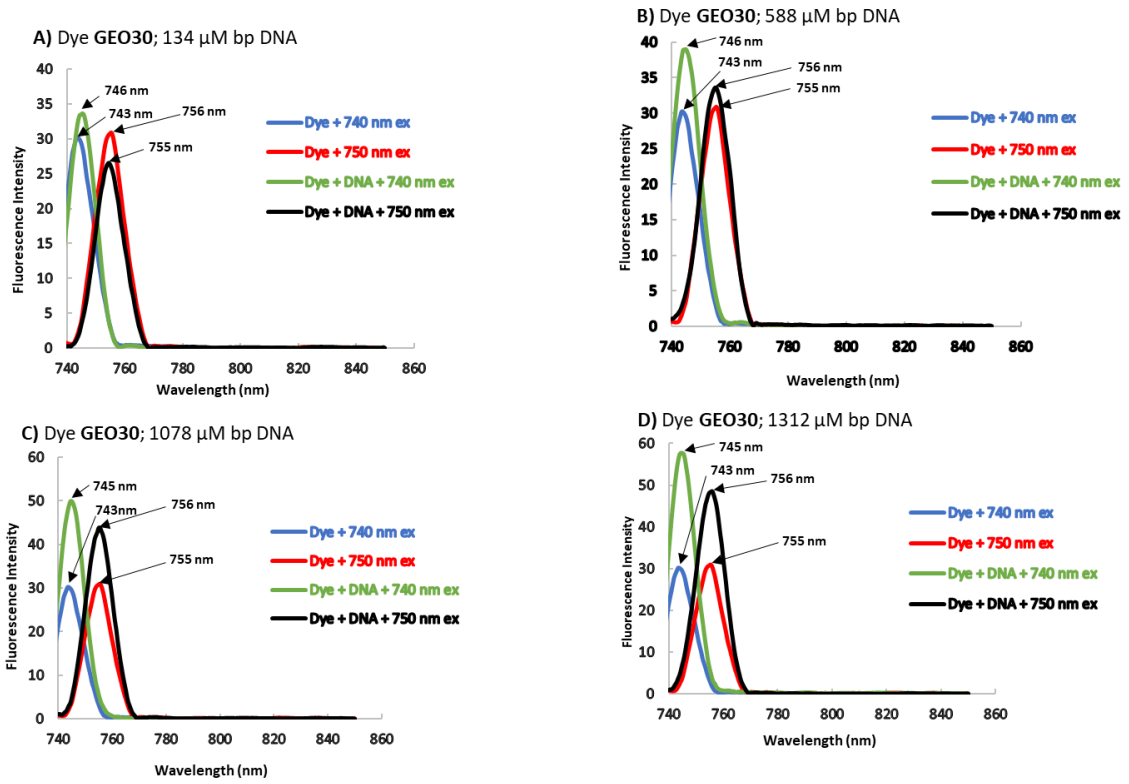

*Figure 13: Fluorescence emission spectra (Em) showing light scattering/fluorescence of 10 µM dye **GEO30** in 10 mM sodium phosphate buffer pH 7.0 (22 °C) in the presence and absence of: (A) 134 µM bp CT DNA; (B) 588 µM bp CT DNA; (C) 1078 µM bp CT DNA; and (D) 1312* µM *bp CT DNA bp CT DNA. Emission spectra were recorded at excitation wavelengths (E_X) 740 and 750 nm.*

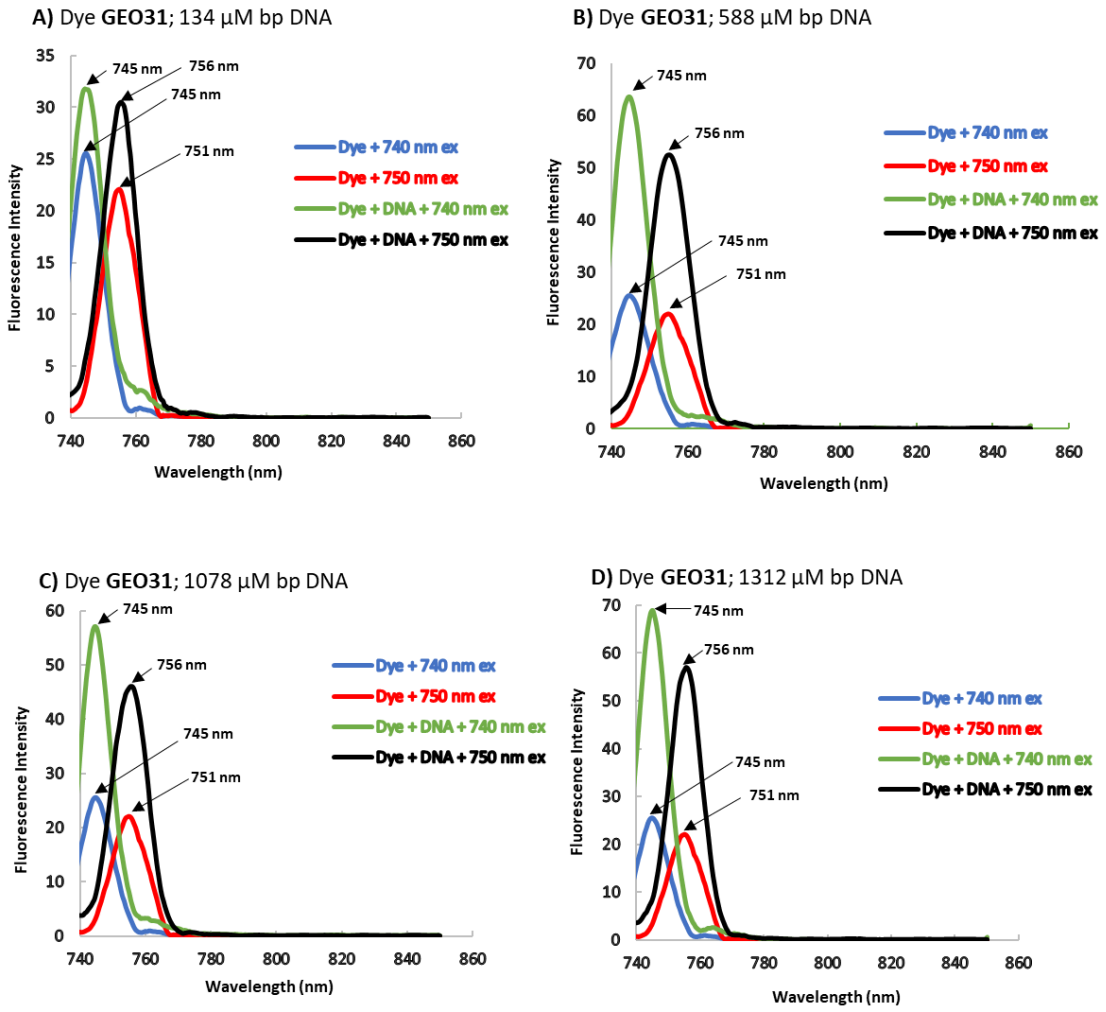

*Figure 14: Fluorescence emission spectra (Em) showing light scattering/ fluorescence of 10 µM dye **GEO31** in 10 mM sodium phosphate buffer pH 7.0 (22 °C) in the presence and absence of: (A) 134 µM bp CT DNA; (B) 588 µM bp CT DNA; (C) 1078 µM bp CT DNA; and (D) 1312 µM bp CT DNA. Emission spectra were recorded at various excitation wavelengths (E_X) 740 and 750 nm*

2.3.5 Competitive DNA Binding

In this experiment, competitive DNA binding assays of dye **GEO30** and **GEO31** were carried out to ascertain the DNA binding modes. UV-visible spectroscopic spectra were recorded to analyze aqueous solutions of dye **GEO30** or **GEO31** alone and with untreated CT DNA compared to solutions containing CT DNA pre-equilibrated with known minor groove binder pentamidine or major groove binder methyl green.[24-26] Upon the addition of pentamidine as

shown in Figures 2.10A and 2.10B, it is observed that the pentamidine disrupts complex formed between DNA duplex structure and **GEO30** as well as **GEO31**. This is evident because the addition of pentamidine shifts the λ_{max} value of the DNA-**GEO30** complex from ≈ 753 nm to ≈ 742 nm, a value approaching free dye (Figure 2.10A). In the case of **GEO31**, pentamidine causes the dye's absorption to decrease shifting the λ_{max} of the DNA-**GEO31** complex from ≈ 749 nm to ≈ 742 nm, a value approaching free dye (Figure 2.10B). This indicates that there might be some direct interaction between pentamidine and the DNA in a way that blocks the dyes from binding. Since the DNA-dye complex is reverting back to the dye only form, it is possible that pentamidine might be decreasing the number of dye-accessible minor groove binding sites on the DNA.

When methyl green was added, the shoulder present in the DNA-dye complex of dye **GEO30** also disappeared, also suggesting that the methyl green is preventing the dye from binding to DNA (Figure 2.10C). The absorption value of the DNA-dye complex shifts from ≈ 753 nm to the dye only λ_{max} of ≈ 743 nm. Similarly, the addition of methyl green to DNA-**GEO31** solutions appears to cause a hypochromic shift from ≈ 749 nm to the dye only λ_{max} of ≈ 737 nm (Figure 2.10D). Results suggest that methyl green also has an interaction with DNA, thus allowing for fewer dye-accessible binding sites in the major groove of the DNA.

In summary, since **GEO30** and **GEO31** exhibits changes in the DNA-dye complex in the presence of minor groove binder pentamidine and major groove binder methyl green, our results suggests the dyes interacts with both the minor and major groove of DNA.

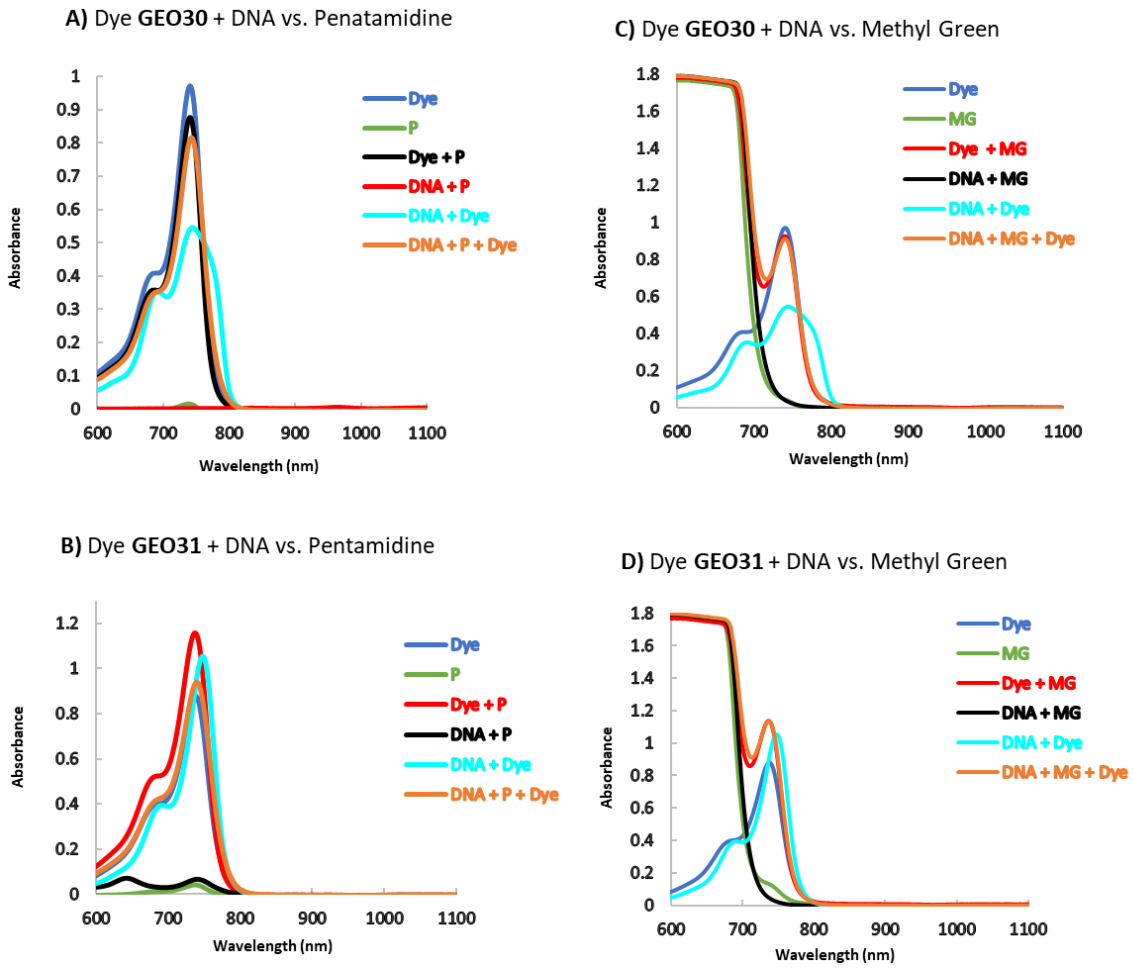

*Figure 15: UV-visible absorption spectra of dye **GEO30** and **GEO31**. All samples contained 10 mM sodium phosphate buffer pH 7.0 (22 °C) and one or more of the following: 10 µM of dye **GEO30** or **GEO31**, 150 µM bp of CT DNA, and 250 µM of pentamidine or methyl green. Abbreviations: P, pentamidine; MG, methyl green.*

2.3.6 ROS Mechanism by Regent-Induced Changes in Dye-sensitized Photocleavage

The ROS mechanism that induces DNA photocleavage was investigated utilizing chemical additives. Direct DNA strand cleavage by the dye GEO30 and GEO31 was modified using three chemical agents: sodium benzoate, a type I hydroxyl radical scavenger (•OH), the metal chelating agent ethylenediaminetetraacetic acid (EDTA), and deuterium oxide (D_2O), which increases the life of singlet oxygen.[27] Reaction solutions were irradiated at 750 nm with a LED medical lamp and contained one or more of the following: 10 mM sodium phosphate buffer

pH 7.0, 38 µM bp pUC19 plasmid DNA in the absence and presence of 30 µM dye **GEO30** or **GEO31**, 100 mM sodium benzoate, 100 mM EDTA, and 79% D_2O (*v/v*).

When comparing the photocleavage of **GEO30** and **GEO31** in the absence of chemical additives (Lane 4 in Figure 2.11A, B) to the ones containing chemical additives, there was a noticeably decrease in photocleave yields. In both dyes, sodium benzoate showed a significant decrease in the DNA cleavage yield (Lane 5 in Figure 2.11A, B). The metal chelating agent EDTA is known for its ability to interrupt the Fenton reaction by chelating trace levels of iron and copper ions present in deionized distilled water. When EDTA was added to **GEO30** and **GEO31** photocleavage reactions, Figure 2.11A, B (Lane 7), there was also inhibition of DNA strand breaks. This points to Fenton chemistry as a possible hydroxyl radical source as shown in the mechanism in Figure 2.12. [18, 19] In these multistep reactions, the reduced photosensitizer triplet state ($^3PS^{\bullet -*}$) of dye GEO**30** or **GEO31** interacts with ground state triplet oxygen $^3O_2$ through Type 1 electron transfer to generate superoxide anion radicals ($O_2^{\bullet -}$) (Line 1). Then, through spontaneous dismutation of the $O_2^{\bullet -}$, an H_2O_2 intermediate is formed, which in the presence of Fe(II) results in the generation of hydroxyl radicals ($OH^{\bullet}$) via Fenton reaction (Lane 3 and 4).[18, 19]

We then studied for the involvement of an alternate ROS pathway involving DNA damage by Type 2 singlet oxygen ($^1O_2$). Towards this end, we replaced H_2O with 79% D_2O (*v/v*). Deuterium oxide increases the lifetime of singlet oxygen by a 10-fold, which would increase DNA cleavage if singlet oxygen were generated.[20, 21] However, D_2O did not enhance DNA strand cleavage significantly as observed in Figure 2.11A, B (Lane 9). Therefore, it is unlikely that Type 2 singlet oxygen plays a major role in dye **GEO30** or **GEO31** sensitized DNA photocleavage.

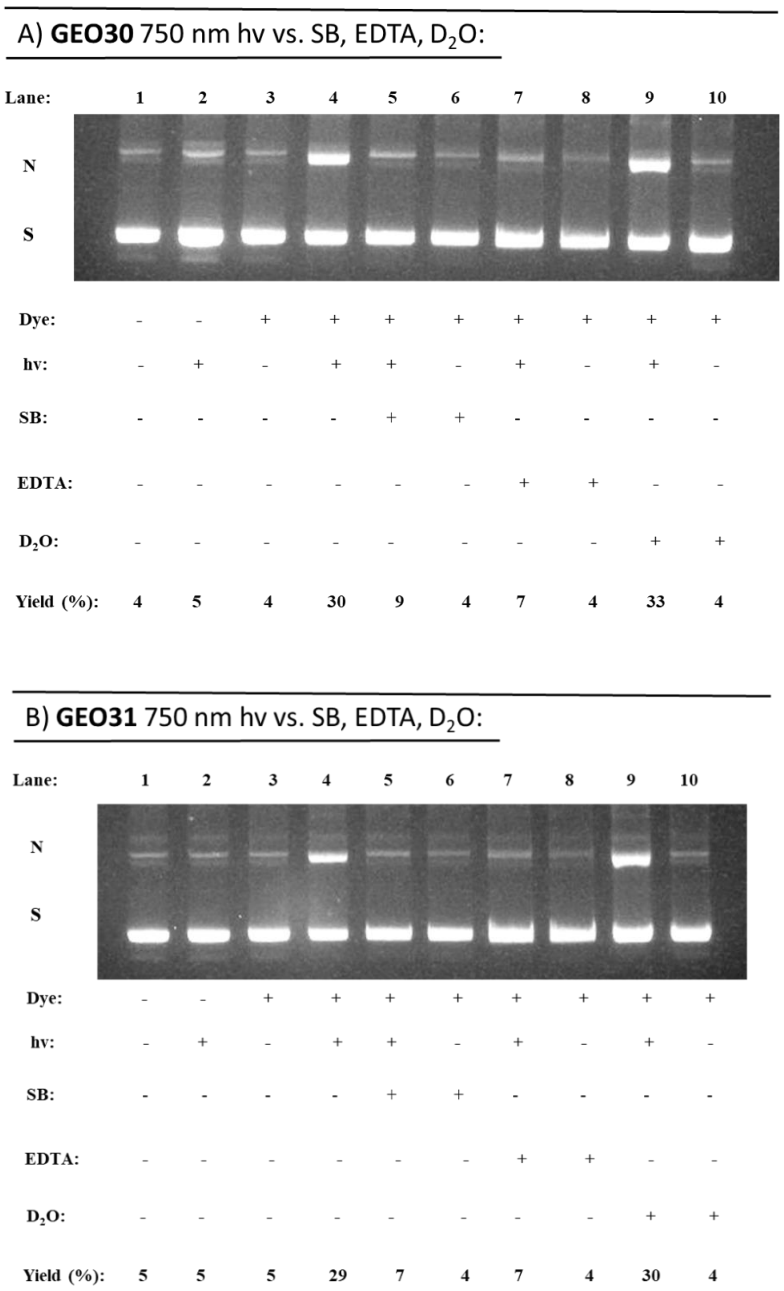

Figure 16: Representative agarose gels comparing levels of dye-sensitized photocleavage of pUC19 plasmid DNA by dyes: (A) ***GEO30*** *and (B)* ***GEO31****. Reaction solutions were irradiated at 750 nm LED medical lamp and contained one or more of the following: 10 mM sodium phosphate buffer pH 7.0, 38 µM bp pUC19 plasmid DNA in the absence and presence of 30 µM dye* ***GEO30*** *or* ***GEO31****, 100 mM sodium benzoate, 100 mM EDTA, and 79 % D_2O (v/v). Abbreviations: N = nicked; S = supercoiled.*

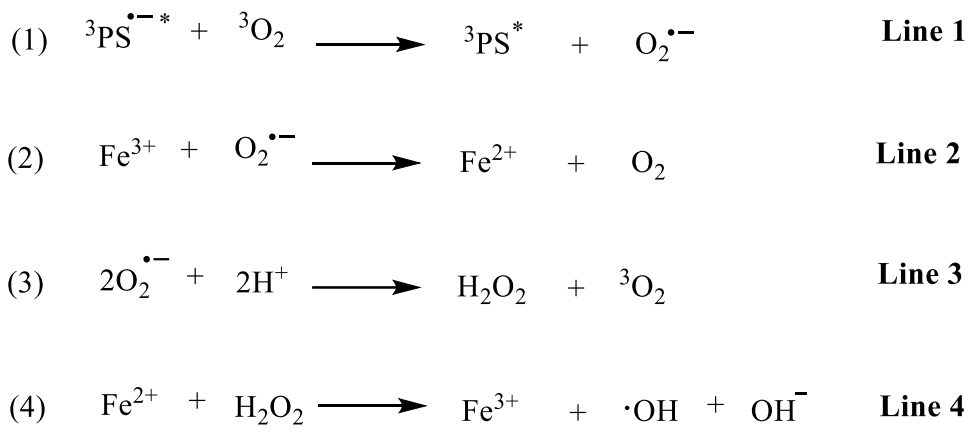

*Figure 17: A plausible mechanism of the ability of **GEO30** and **GEO31** to sensitize DNA via hydroxyl radical formation.* [18, 19]

2.3.7 ROS Detection by HPF Fluorescent Probe

In this experiment, we attempted to detect hydroxyl radicals and singlet oxygen using the fluorescent probe 3'-(4-hydroxyphenyl) fluorescein (HPF). The reactions contained 10 mM sodium phosphate buffer pH 7.0 in the presence and absence of 0.5 µM of dyes **GEO30** or **GEO31**, 3 mM of HPF, 100 mM sodium benzoate, and 90% D_2O (*v/v*). Each reaction was kept in the dark (22 °C) or irradiated for 30 min using a 750 nm LED medical lamp. Fluorescence emission spectra were recorded using HPF's excitation wavelengths of 490 nm (Figure 2.13).

The dyes in the dark do not generate an HPF signal. However, when dye **GEO30** or **GEO31** is introduced and subsequently irradiated at 750 nm, a maximum fluorescence emission intensity was generated, which was an indication of ROS production (Figure 2.13A, B). Additionally, when the hydroxyl radical scavenger sodium benzoate was added to the solutions, the fluorescent intensity decreased implying that sodium benzoate quenched the production of hydroxyl radicals (Figure 2.13A, B). This finding is in agreement with the dye **GEO30** and **GEO31** scavenger DNA photocleavage experiment using sodium benzoate (Figure 2.11A, B),

which suggests that hydroxyl radicals play a major role in the DNA cleavage by dyes **GEO30** and **GEO32**. The mechanism of action of HPF is depicted in Figure 2.14.

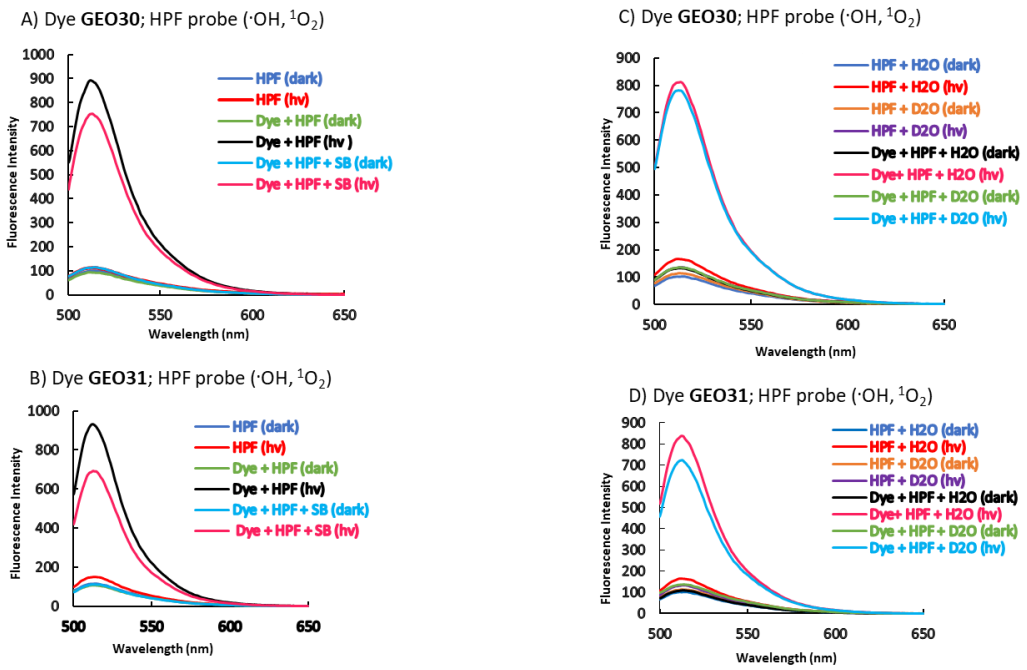

Figure 18: *Fluorescence emission spectra depicting ROS production by dye **GEO30** and **GEO32**. Emission spectra were recorded for solutions containing 10 mM sodium phosphate buffer pH 7.0 and: (A, B) 0.5 µM dye, 3 mM of hydroxyphenyl fluorescein (HPF), 100 mM sodium benzoate (SB) excitation and emission wavelengths E_X/Em = 490/500 nm; (B, C) 0.5 µM dye, or in 100 % H_2O or 90 % deuterium oxide (D_2O) (v/v) with E_X/E_m = 490/500 nm. Reactions were kept in the dark or irradiated at 750 nm for 30 min (22 °C).*

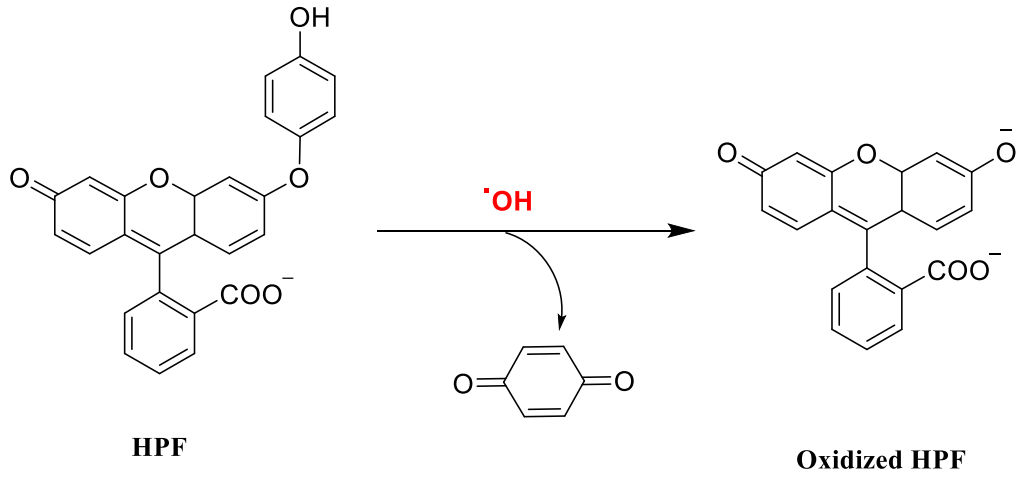

Figure 19: Mechanism of action of 3'-(4-hydroxyphenyl) fluorescein (HPF) illustrating how HPF alone is non-fluorescent but is converted to a fluorescent compound when oxidized by hydroxyl radicals.

In Figure 2.13C and 2.13D, we investigated the involvement of type II singlet oxygen by replacing H_2O with 90 % D_2O (*v/v*). The data showed that D_2O did not enhance or improve the fluorescence signal of dyes **GEO30** or **GEO31** compared to H_2O. This result was in line with the DNA photocleavage (Figure 2.11A, B), which showed marginal increase of DNA cleavage in the presence of D_2O.

2.4 Supplementary Information

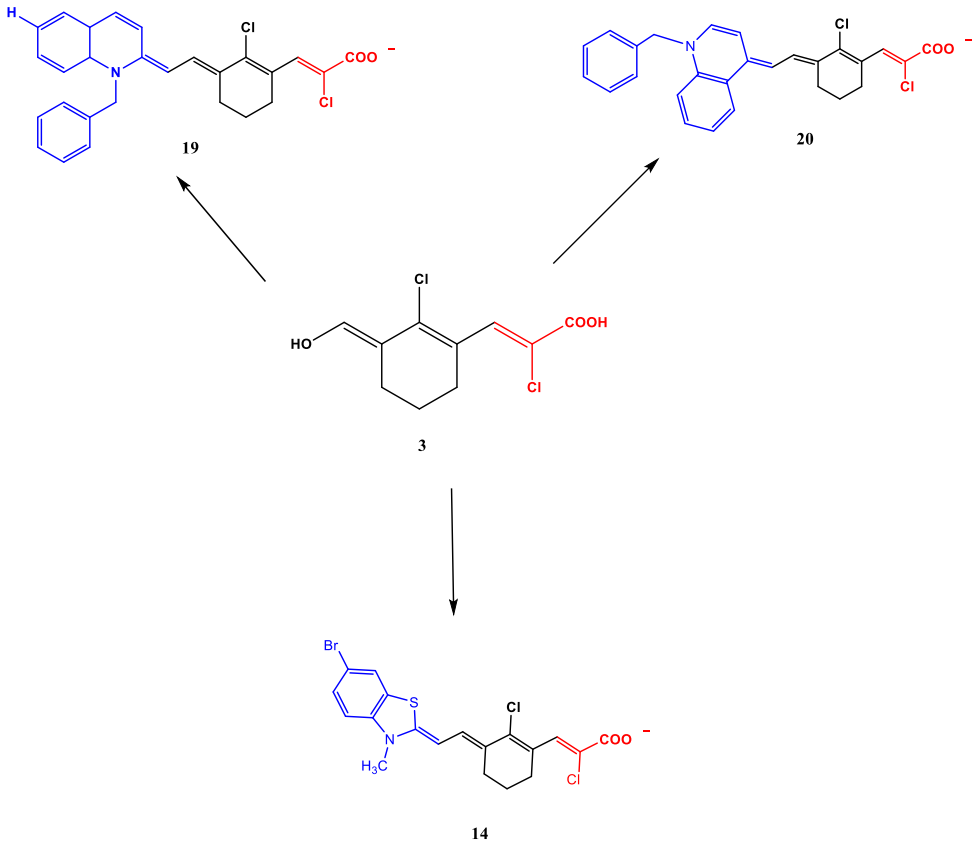

*Figure 20: Donor acceptor fluorophores: **14**, **19**, and **20** with a benzothiazole, 2-quinolium, and 4-quinolium donor groups, respectively were also investigated for their photo-stability in various solvents and for their photocleavage activities. Significant levels of DNA photocleavage were not observed.*[1]

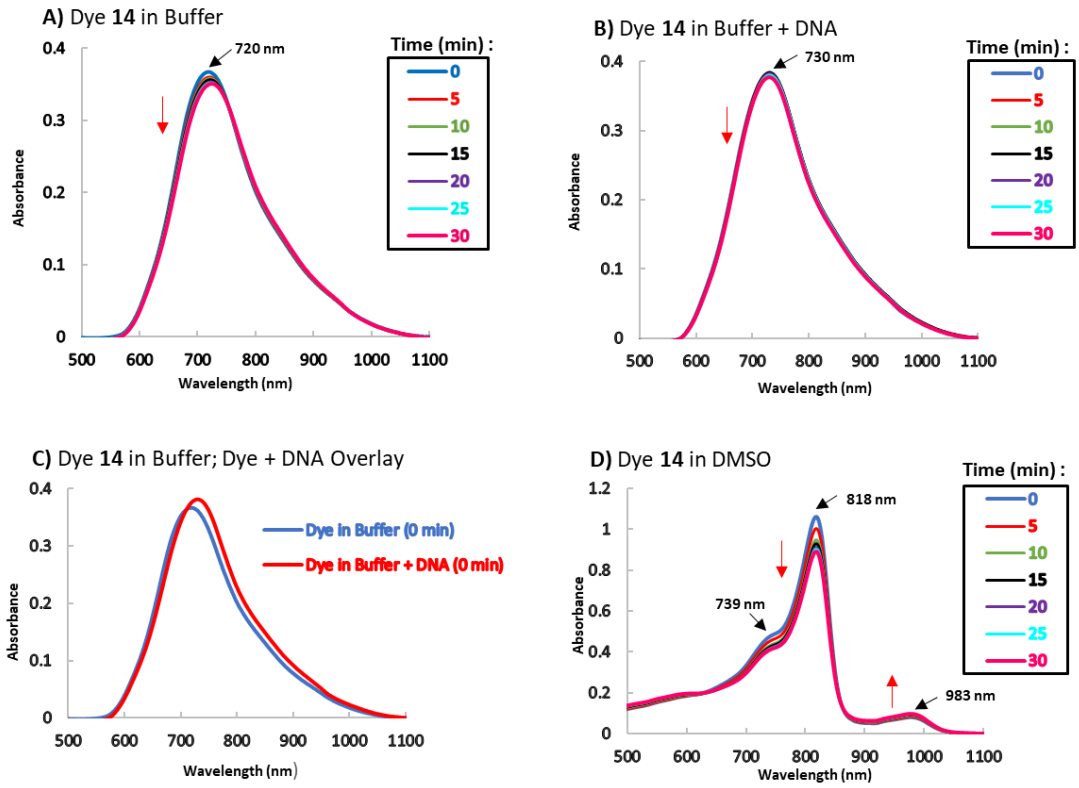

*Figure 21: Time course spectra for 10 µM of compound **14**: in the absence (A) and in the presence (B) of 150 µM bp CT DNA using a working concentration of 10 mM sodium phosphate buffer (pH =7), (C) the effect of DNA on dye using 0-min time point spectra, (D) compound **14** in DMSO showing the relative stability of the dye in a solvent less polar than water.*

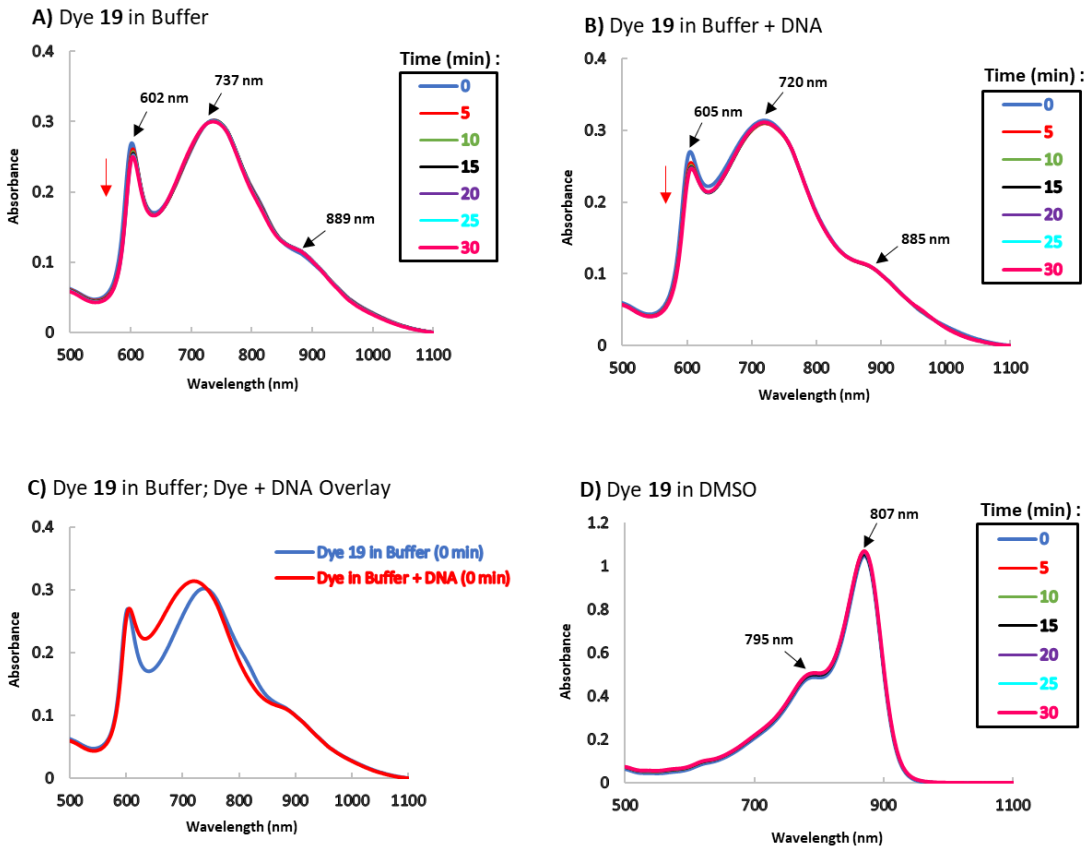

Figure 22: *Time course spectra for 10 µM of compound **19**: in the absence (A) and in the presence (B) of 150 µM bp CT DNA using a working concentration of 10 mM sodium phosphate buffer (pH =7), (C) the effect of DNA on dye using 0-min time point spectra, (D) compound **19** in DMSO showing the relative stability of the dye in a solvent less polar than water.*

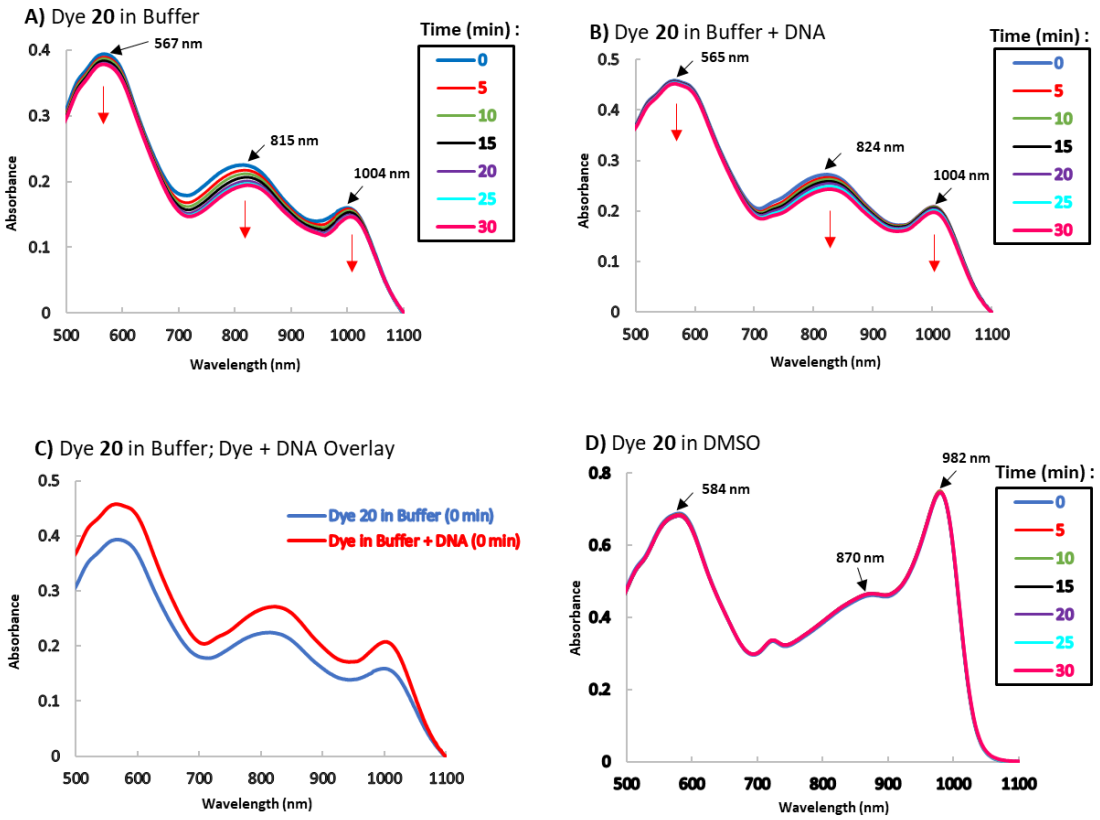

*Figure 23: Time course spectra for 10 µM of compound **20**: in the absence (A) and in the presence (B) of 150 µM bp CT DNA using a working concentration of 10 mM sodium phosphate buffer (pH =7), (C) the effect of DNA on dye using 0-min time point spectra, (D) compound **20** in DMSO showing the relative stability of the dye in a solvent less polar than water.*

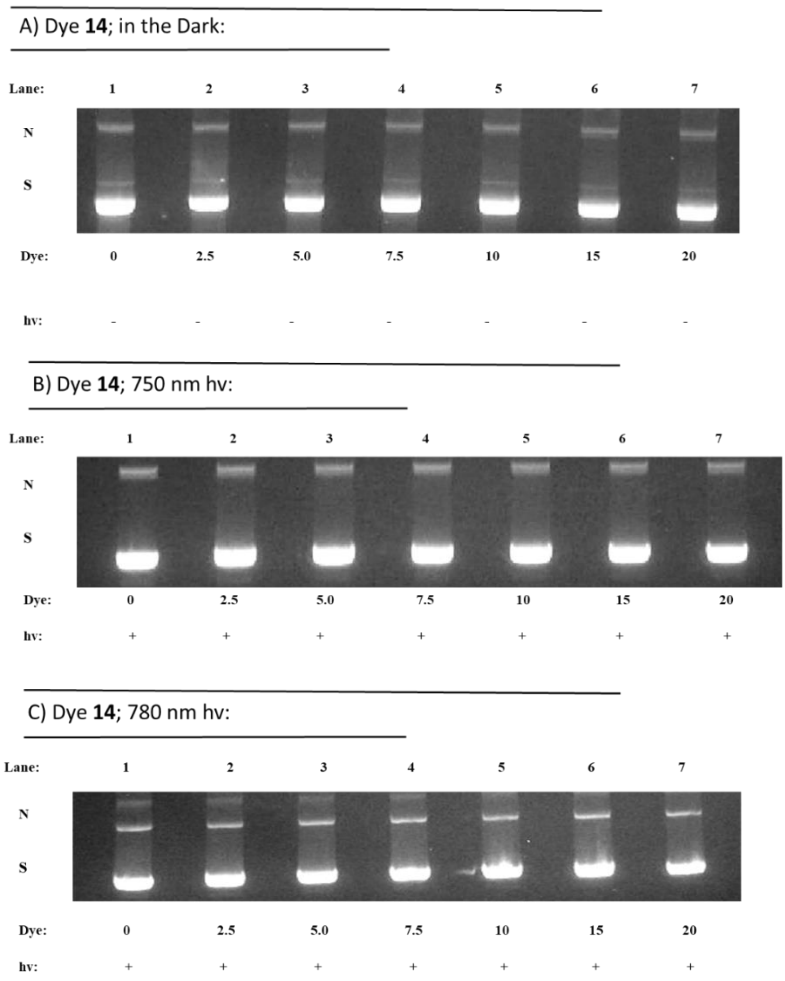

*Figure 24: Representative dye-sensitized photocleavage of pUC19 plasmid DNA by compound **14** in 1.5 % agarose gels. Reactions contained 10 mM sodium phosphate buffer pH 7.0, 38 µM bp pUC19 plasmid DNA in the absence and presence of 0-20 µM dye. Each reaction was either kept in the dark or irradiated for 30 min with a 750 nm LED medical lamp and 780 nm LED laser. A metal block was used to hold the samples and was emersed in an ice bath during the reaction. Abbreviations: N, nicked; S, supercoiled.*

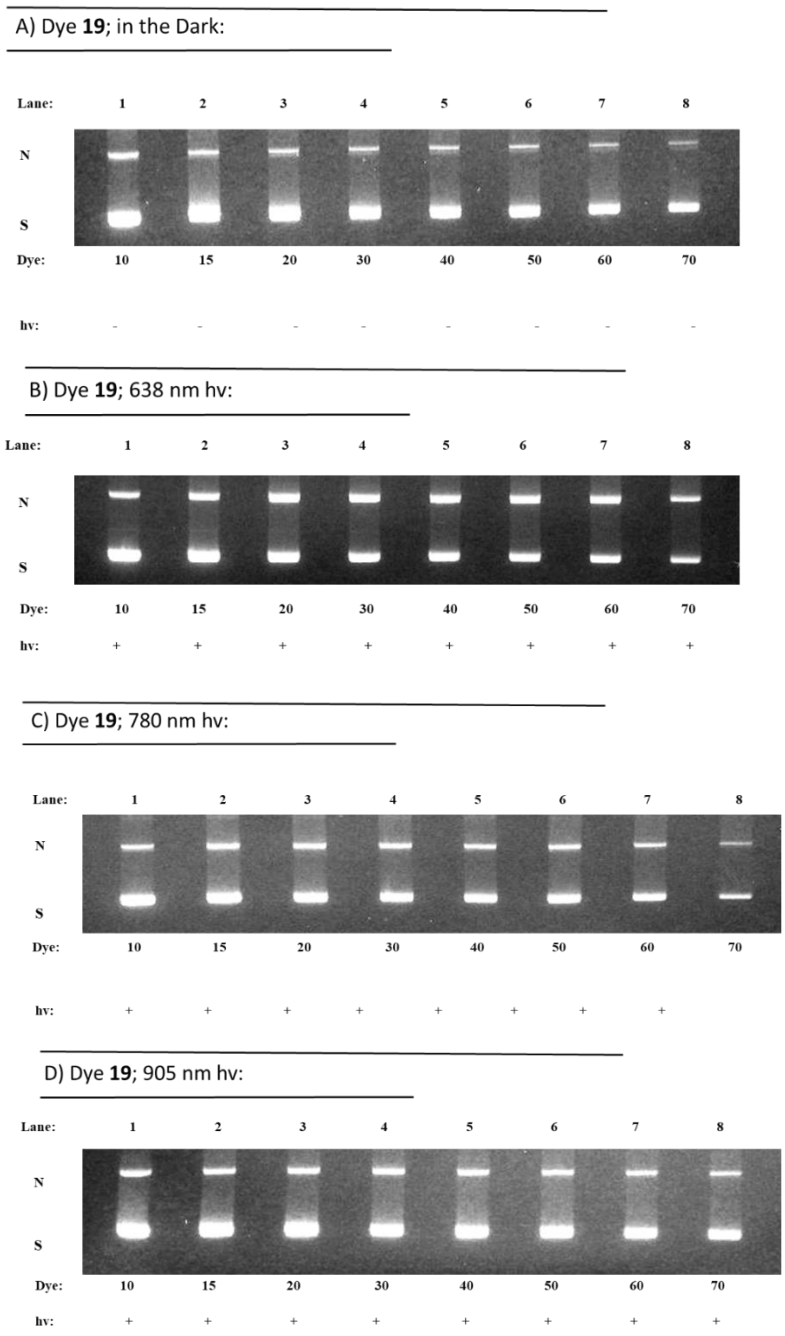

*Figure 25: Representative dye-sensitized photocleavage of pUC19 plasmid DNA by compound **19** in 1.5 % agarose gels. Reactions contained 10 mM sodium phosphate buffer pH 7.0, 38 µM bp pUC19 plasmid DNA in the absence and presence of 0-20 µM dye. Each reaction was either kept in the dark or irradiated for 30 min with a 638, 780, and 905 nm LED laser. A metal block was used to hold the samples and was emersed in an ice bath during the reaction. Abbreviations: N, nicked; S, supercoiled.*

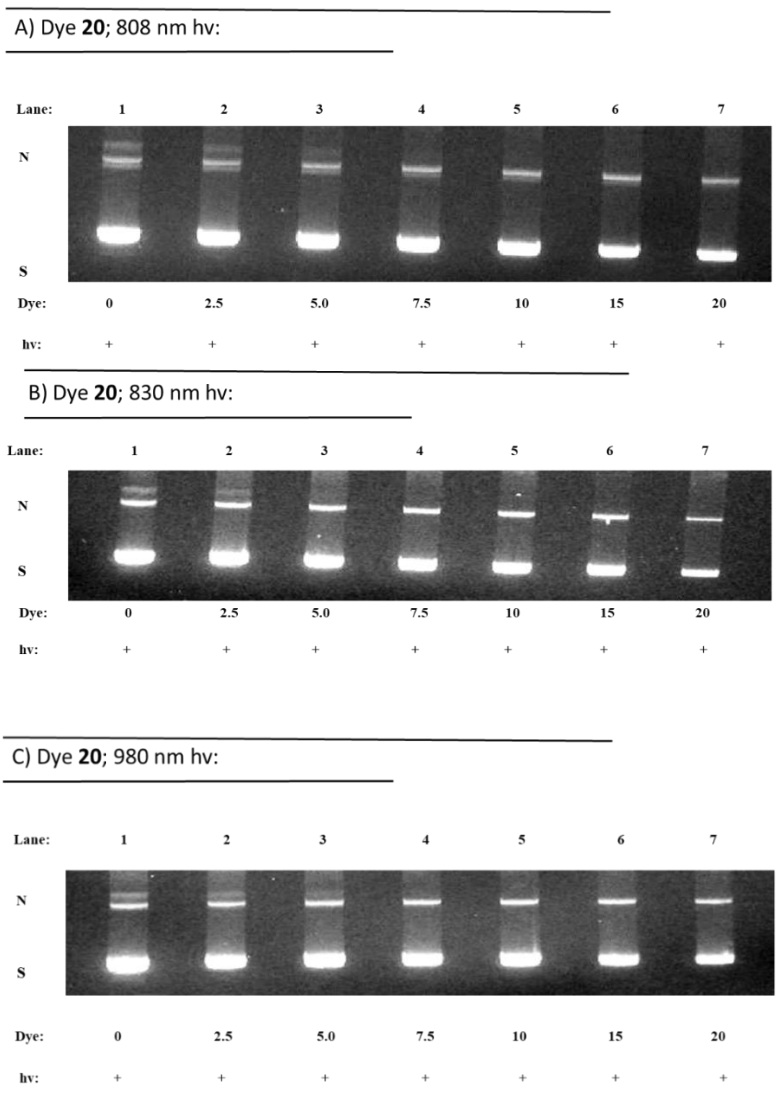

*Figure 26: Representative dye-sensitized photocleavage of pUC19 plasmid DNA by compound **20** in 1.5 % agarose gels. Reactions contained 10 mM sodium phosphate buffer pH 7.0, 38 μM bp pUC19 plasmid DNA in the absence and presence of 0-20 μM dye. Each reaction was either kept in the dark or irradiated for 30 min with an 808, 830, and 980 nm LED laser. A metal block was used to hold the samples and was emersed in an ice bath during the reaction. Abbreviations: N, nicked; S, supercoiled.*

2.5 References

1. Essam, Z. M.; Ozmen, G. E.; Setiawan, D.; Hamid, R. R.; Abd El-Aal, R. M.; Aneja, R.; Hamelberg, D.; Henary, M. Donor Acceptor Fluorophores: Synthesis, Optical Properties, TD-DFT and Cytotoxicity Studies. *Organic & Biomolecular Chemistry* **2021**, *19* (8), 1885-1846.
2. Armitage, B. A. Cyanine Dye–DNA Interactions: Intercalation, Groove Binding, and Aggregation. *In DNA Binders and Related Subjects* **2005**; pp 55-76.
3. Kawabe, Y.; Kato, S. J. D. Pigments, Spectroscopic Study of Cyanine Dyes Interacting with the Biopolymer, DNA. *Dyes and Pigments* **2012,** *95*, 614-618.
4. Garoff, R. A.; Litzinger, E. A.; Connor, R. E.; Fishman, I.; Armitage, B. A. Helical Aggregation of Cyanine Dyes on DNA Templates: Effect of Dye Structure on Formation of Homo- and Heteroaggregates. *Langmuir* **2002,** *18* (16), 6330-6337.
5. Wang, M.; Silva, G. L.; Armitage, B. A. DNA-Templated Formation of a Helical Cyanine Dye J-Aggregate. *Journal of American Chemical Society* **2000,** *122* (41), 9977-9986.
6. Jacques, S. L., Optical Properties of Biological Tissues: A Review. *Physics in Medicine and Biology* **2013,** *58* (11), R37-61.
7. Ormond, A. B.; Freeman, H. S. Dye Sensitizers for Photodynamic Therapy. *Materials (Basel)* **2013,** *6* (3), 817-840.
8. Li, Z. Y.; Grant, K. B. DNA Photo-Cleaving Agents in the Far-Red to Near-Infrared Range - A Review. *Rsc Advances* **2016,** *6* (29), 24617-24634.
9. Luby, B. M.; Walsh, C. D.; Zheng, G. Advanced Photosensitizer Activation Strategies for Smarter Photodynamic Therapy Beacons. *Angewandte Chemie-International Edition* **2019,** *58* (9), 2558-2569.
10. Bonnett, R. Photosensitizers of the Porphyrin and Phthalocyanine Series for Photodynamic Therapy. *Chemical Society Reviews* **1995,** *24* (1), 19-33.
11. Ochsner, M. Photophysical and Photobiological Processes in the Photodynamic Therapy of Tumours. *Journal of Photochemistry and Photobiology. B, Biology* **1997,** *39* (1), 1-18.
12. Pogozelski, W. K.; Tullius, T. D. Oxidative Strand Scission of Nucleic Acids: Routes Initiated by Hydrogen Abstraction from the Sugar Moiety. *Chemical Reviews* **1998,** *98* (3), 1089-1108.
13. Agostinis, P.; Berg, K.; Cengel, K. A.; Foster, T. H.; Girotti, A. W.; Gollnick, S. O.; Hahn, S. M.; Hamblin, M. R.; Juzeniene, A.; Kessel, D.; Korbelik, M.; Moan, J.; Mroz, P.; Nowis, D.; Piette, J.; Wilson, B. C.; Golab, J. Photodynamic Therapy of Cancer: An Update. *CA: A Cancer Journal for Clinicians* **2011,** *61* (4), 250-81.
14. Kawabe, Y.; Kato, S. J. D. Pigments, Spectroscopic Study of Cyanine Dyes Interacting with the Biopolymer, DNA. *Dyes and Pigments* **2012,** *95*, 614-618.
15. Garoff, R. A.; Litzinger, E. A.; Connor, R. E.; Fishman, I.; Armitage, B. A. Helical Aggregation of Cyanine Dyes on DNA Templates: Effect of Dye Structure on Formation of Homo- and Heteroaggregates. *Langmuir* **2002,** *18* (16), 6330-6337.
16. Wang, M.; Silva, G. L.; Armitage, B. A. DNA-Templated Formation of a Helical Cyanine Dye J-Aggregate. *Journal of American Chemical Society* **2000,** *122* (41), 9977-9986.

17. Seifert, J. L.; Connor, R. E.; Kushon, S. A.; Wang, M.; Armitage, B. A. Spontaneous Assembly of Helical Cyanine Dye Aggregates on DNA Nanotemplates. *Journal of American Chemical Society* **1999**, 121 (13), 2987-2995.
18. Bonnett, R. Photosensitizers of the Porphyrin and Phthalocyanine Series for Photodynamic Therapy. *Chemical Society Reviews* **1995,** *24* (1), 19-33.
19. Ochsner, M. Photophysical and Photobiological Processes in the Photodynamic Therapy of Tumours. *Journal of photochemistry and photobiology. B, Biology* **1997,** *39* (1), 1-18.
20. Williams, D. E.; Fischer, C. M.; Kassai, M.; Gude, L.; Fernández, M.-J.; Lorente, A.; Grant, K. B. An unlikely DNA cleaving agent: A Photo-Active Trinuclear Cu(II) Complex Based on Hexaazatriphenylene. *Journal of Inorganic Biochemistry* **2017,** *168*, 55-66.
21. Merkel, P. B.; Kearns, D. R. Radiationless Decay of Singlet Molecular Oxygen in Solution. Experimental and Theoretical Study of Electronic-to-Vibrational Energy Transfer. *Journal of American Chemical Society* **1972,** *94* (21), 7244-7253.
22. Basnet, K.; Fatemipouya, T.; St. Lorenz, A.; Nguyen, M.; Taratula, O.; Henary, M.; Grant, K. B. Single Photon DNA Photocleavage at 830 Nm by Quinoline Dicarbocyanine Dyes. *Chemical Communications* **2019**, *55* (84), 12667–12670.
23. Clarke, R. J.; Oprysa, A. Fluorescence and Light Scattering. *Journal of Chemical Education* **2004,** *81* (5), 705.
24. Edwards, K. J.; Jenkins, T. C.; Neidle, S. Crystal Structure of a Pentamidine-Oligonucleotide Complex: Implications for DNA-Binding Properties. *Biochemistry* **1992,** *31* (31), 7104-9.
25. Kim, S. K.; Nordén, B. Methyl green. A DNA Major-Groove Binding Drug. *FEBS Letters* **1993,** *315* (1), 61-4.
26. Prieto, D.; Aparicio, G.; Morande, P. E.; Zolessi, F. R. A Fast, Low Cost, and Highly Efficient Fluorescent DNA Labeling Method using Methyl Green. *Histochemistry and cell biology* **2014,** *142* (3), 335-45.
27. Prasad, A.; Sedlářová, M.; Pospíšil, P. Singlet Oxygen Imaging using Fluorescent Probe Singlet Oxygen Sensor Green in Photosynthetic Organisms. *Scientific Reports* **2018,** *8* (1), 13685.
28. Zepp, R. G.; Faust, B. C.; Hoigne, J. Hydroxyl Radical Formation in Aqueous Reactions (pH 3-8) of Iron(II) with Hydrogen Peroxide: The Photo-Fenton Reaction. *Environmental Science & Technology* **1992,** *26* (2), 313-319.

3 MATERIALS AND METHODS

3.1 General

All aqueous solutions for the UV-visible, fluorescence, and DNA photocleavage studies were made with deionized distilled water. Double-stranded circular pUC19 plasmid DNA was cloned from XL-1 blue *E. coli* competent cells (Stratagene, San Diego, CA, USA), isolated, and purified using alkaline lysis and anion exchange chromatography with a QIAfilter Plasmid Mega Kit according to manufacturer's instructions (Qiagen™, Hilden, Germany, Cat. No. 12263). Sodium phosphate buffer (pH = 7.0) used in DNA solutions was prepared from sodium phosphate monobasic and sodium phosphate dibasic salts (Thermo Fisher Scientific, Waltham, MA, USA). Calf thymus DNA (CT DNA) was purchased from Invitrogen (Carlsbad, CA, USA; 10 mg/mL, average size ≤ 2000 bp, Cat. No. 15633-019), deuterium oxide (99.9 %), and agarose were purchased from Cambridge Isotope Laboratories and Bio-Rad. All other reagents, including sodium benzoate (99 %), dimethyl sulfoxide (DMSO, ≥ 99.99 %), ethidium bromide, pentamidine isethionate salt, methylene blue, and methyl green (92%) were provided by Sigma-Aldrich (St. Louis, MO, USA). UV–visible absorption and fluorescence emission spectra were measured using PerkinElmer Lambda 35 (PerkinElmer, Waltham, MA, USA) and a PerkinElmer LS55 spectrophotometers (PerkinElmer, Waltham, MA, USA).

3.2 UV-Visible Spectroscopy

The UV-visible absorption time-course spectra of dyes **GEO30**, **GEO32**, **GEO31** and **GEO1** were measured using a PerkinElmer Lambda 35 spectrophotometer. The solutions in the cuvettes contained 10 μM of the dye in either 10 mM sodium phosphate pH 7.0 (22 °C) in the absence and presence of 150 μM bp CT DNA or in DMSO with a final volume of 500 μL. The absorption spectra were recorded at a time intervals from 0 to 30 min. All titration absorption

spectra were adjusted for baseline drift. In the UV-visible DNA titration experiment of dye **GEO30** and **GEO31**, small volumes of an aqueous solution of 16,905 µM bp CT DNA were sequentially added to samples containing 10 µM dye **GEO30** or **GEO31** in 10 mM sodium phosphate pH 7.0 with an initial volume of 500 µL and final volume of 549 µL. Final concentrations of CT DNA present in the sample ranged from 33 µM bp up to 1539 µM bp. All titration absorption spectra were adjusted for sample dilution.

3.3 DNA Photocleavage

The DNA photocleavage reactions consisted of various concentrations (0-70 µM) of dyes **GEO30**, **GEO32**, **GEO31,** or **GEO1**, 10 mM of sodium phosphate (pH 7.0), 38 µM bp of pUC19 plasmid DNA with a total volume of 40 µL. The Eppendorf tubes containing the reaction solutions were kept in a metal block that was emersed in an ice bath. Samples were kept in the dark or irradiated for 30 min using a 750 nm LED medical lamp or 780 nm LED laser. After the irradiation period, 3 µL of loading buffer containing 15.0% (*w*/*v*) ficoll and 0.025% (*w*/*v*) bromophenol blue were added to each sample and 20 µL of the resulting solution were loaded to the wells of 1.5 % agarose gel containing 5 mg/µL ethidium bromide. Then, ethidium bromide (5 mg/µL, final concentration) was added to 650 mL of 1 × tris-acetate-EDTA (TAE) running buffer. The reactions were electrophoresed for 60 min at 100 V in a Bio-Rad Laboratories gel box. The gels were then visualized at 302 nm with a VWR Scientific LM-20E transilluminator, photographed with a UVP PhotoDoc-It™ Imaging System and quantitated using ImageJ software. DNA photocleavage yield were calculated using the following formula: Percent Photocleavage (%) = [(Linear + Nicked DNA)/(Linear + Nicked + Supercoiled DNA)] × 100.

3.4 Fluorescence Spectrophotometry

Fluorescence of dye **GEO30** and **GEO31** were measured at 22 °C with PerkinElmer LS55 spectrophotometer. Solutions contained 10 mM sodium phosphate buffer (pH 7.0) and 10 µM of dye **GEO30** or **GEO31** in the absence or presence of 134, 588, 1078, or 1312 µM bp CT DNA. Samples were prepared in 3.0 mL Starna quartz cuvettes (2000 µL, final volume). The samples were then excited at 740 nm and 750 nm and emission spectra were recorded (22 °C). The scan speed of the spectrophotometer was 100 nm/min, gain was set at medium, and the excitation and emission slit widths were 4.5 nm.

3.5 Competitive DNA Binding Mode

In the competitive DNA binding, UV- visible spectroscopy was employed to measure the absorbance of dye **GEO30** or **GEO31** with pentamidine and methyl green. The solutions in the cuvettes contained 10 mM of sodium phosphate buffer pH 7.0 (22 °C), in the absence and presence of 150 µM bp pUC19 plasmid DNA, 10 µM of dye **GEO30** or **GEO31**, and 250 µM of pentamidine or methyl green (500 µL, total volume).

3.6 Regent-Induced Changes in Dye-sensitized Photocleavage

The reaction solutions consisted of 10 mM of sodium phosphate buffer pH 7.0, 38 µM bp pUC19 plasmid DNA and 30 µM of dye **GEO30 or GEO31** in the absence and presence of 100 mM of sodium benzoate, 100 mM EDTA, or 79 % D_2O (*v/v*) with a total volume of 40 µL. The reactions were then irradiated with a 750 nm LED medical lamp for 30 min in an ice bath. After the irradiation period, the reactions were electrophoresed on 1.5 % non-denaturing agarose gel, visualized, and quantitated as mentioned previously.

3.7 ROS Detection by HPF Fluorescent Probe

Reactions contained 10 mM of sodium phosphate buffer pH 7.0, and 0.5 µM of dye **GEO30** or **GEO31** in the absence and presence of 3 mM of HPF, 100 mM of sodium benzoate, 100 mM EDTA, or 90 % D_2O (*v/v*) with final volume of 1500 µL. The reactions were kept in the dark or irradiated with a 750 nm LED medical lamp for 30 min. After the irradiation, the fluorescence emission spectra were recorded by exciting the sample at 490 nm and recording HPF emission from 500 nm to 800 nm.

4 CONCLUSION AND FUTURE DIRECTION

Photosensitizing agents that can be light activated in the near-infrared phototherapeutic window are of a great importance for photodynamic therapy, by allowing an enhanced penetration depth of the incident light through biological tissues. In this study, we showed that two asymmetrical donor acceptor fluorophores (**GEO30** and **GEO31**) containing an indole donor moiety and a neutral charge at pH 7.0 cleaved DNA in the near-infrared range. UV-visible spectra of the dyes revealed that DNA has a major effect on dye aggregation. Increasing DNA concentrations induced the formation of a bathochromic and hypochromic DNA complexes with **GEO30** and **GEO31**. Competitive DNA binding results suggested that dyes **GEO30** and **GEO31** might bind in the minor and major groove of DNA. DNA photocleavage experiments of the dyes with chemical additives and analyses of dye solutions in the absence and presence of HPF fluorescent probe, showed that irradiation of the free and DNA-bound form of dyes **GEO30** and **GEO31** with a 750 nm LED medical lamp generates Type I $^{\bullet}OH$ radicals that can cleave plasmid DNA in good yield.

A future direction of this work includes studying the photocytotoxic effects of dyes **GEO30** and **GEO31.** In addition, we plan to investigate positive donor acceptor fluorophores that absorb light in the near-infrared wavelength range in an effort to discover phototherapeutic agents suitable for photodynamic therapy. Utilizing near-infrared light has the advantage of deeper tissue penetration through biological tissue, resulting enhanced efficacy of PDT agents in the treatment of cancer and other diseases. Our findings suggest that dyes **GEO30** and **GEO31** could be important as photosensitizing agents in the future of photodynamic therapy.